MICROCOPY RESOLUTION TEST CHART
NATIONAL BUREAU OF STANDARDS-1963-A

AD A090955

A TWO-DIMENSIONAL COMPUTATION OF RIBBED PIPE FLOW

J. Douglas Beason · C.E. Needham

April 1980

Final Report

Approved for public release; distribution unlimited.

DTIC
ELECTED
OCT 3 0 1980

A

Prepared for

Director
DEFENSE NUCLEAR AGENCY
Washington, DC 20305

AIR FORCE WEAPONS LABORATORY
Air Force Systems Command
Kirtland Air Force Base, NM 87117

DDC FILE COPY

80 10 24 034

This final report was prepared by the Air Force Weapons Laboratory, Kirtland Air Force Base, New Mexico, under Job Order WDNB4406. Lieutenant J. Douglas Beason (NTESB) was the Laboratory Project Officer-in Charge.

When US Government drawings, specifications, or other data are used for any purpose other than a definitely related Government procurement operation, the Government thereby incurs no responsibility nor any obligation whatsoever, and the fact that the Government may have formulated, furnished, or in any way supplied the said drawings, specifications, or other data, is not to be regarded by implication or otherwise, as in any manner licensing the holder or any other person or corporation, or conveying any rights or permission to manufacture, use, or sell any patented invention that may in any way be related thereto.
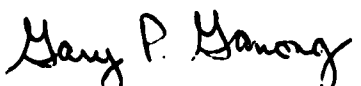
This report has been authored by an employee of the United States Government. The United States Government retains a nonexclusive, royalty-free license to publish or reproduce the material contained herein, or allow others to do so, for United States Government purposes.
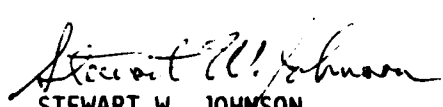
This report has been reviewed by the Public Affairs and is releasable to the National Technical Information Service (NTIS). At NTIS, it will be available to the general public, including foreign nations.

This technical report has been reviewed and is approved for publication.

J. DOUGLAS BEASON
1st Lieutenant, USAF
Project Officer

FOR THE DIRECTOR

GARY P. GANONG   STEWART W. JOHNSON
Lt Colonel, USAF   Lt Colonel, USAF
Chief, Technology and Applications   Chief, Civil Engineering Research
  Branch   Division

DO NOT RETURN THIS COPY. RETAIN OR DESTROY.

REPORT DOCUMENTATION PAGE		READ INSTRUCTIONS BEFORE COMPLETING FORM
1. REPORT NUMBER AFWL-TR-79-65	2. GOVT ACCESSION NO. AD-A0909 55	3. RECIPIENT'S CATALOG NUMBER
4. TITLE (and Subtitle) A TWO-DIMENSIONAL COMPUTATION OF RIBBED PIPE FLOW		5. TYPE OF REPORT & PERIOD COVERED Final Report
		6. PERFORMING ORG. REPORT NUMBER
7. AUTHOR(s) J. Douglas Beason - C. E. Needham		8. CONTRACT OR GRANT NUMBER(s)
9. PERFORMING ORGANIZATION NAME AND ADDRESS Air Force Weapons Laboratory (NTESB) Kirtland Air Force Base, NM 87117		10. PROGRAM ELEMENT, PROJECT, TASK AREA & WORK UNIT NUMBERS WDNB4406/62704H
11. CONTROLLING OFFICE NAME AND ADDRESS Air Force Weapons Laboratory (NTESB) Kirtland Air Force Base, NM 87117		12. REPORT DATE April 1980
		13. NUMBER OF PAGES 60
14. MONITORING AGENCY NAME & ADDRESS(if different from Controlling Office)		15. SECURITY CLASS. (of this report) UNCLASSIFIED
		15a. DECLASSIFICATION/DOWNGRADING SCHEDULE

16. DISTRIBUTION STATEMENT (of this Report)

Approved for public release; distribution unlimited.

17. DISTRIBUTION STATEMENT (of the abstract entered in Block 20, if different from Report)

18. SUPPLEMENTARY NOTES

This research was sponsored by the Defense Nuclear Agency under Subtask Y99QAXSC355, Work Unit: SGJ, Title: Airblast Environment Definition.

19. KEY WORDS (Continue on reverse side if necessary and identify by block number)

HULL	1-D	Trench	Smooth shock tube
SAP	2-D	Fine zone	
Hydrodynamics	Lagrangian	Coarse zone	
Trough	Eulerian	Ribbed shock tube	

20. ABSTRACT (Continue on reverse side if necessary and identify by block number)

The study of ribbed pipe flow is currently of great interest to several diverse groups. Unlike smooth pipe flow which has been studied in great depth, ribbed pipe flow is relatively new to experimental, analytic and computational research efforts. A recent computer simulation of ribbed pipe flow was made by the Air Force Weapons Laboratory using a two-dimensional, Eulerian finite difference hydrodynamic computer code. Two separate experiments were modeled using a course (0.13 cm x 0.78 cm) and a very fine (0.065 cm x 0.065 cm) zone

(over)

20. ABSTRACT (Cont'd)

calculation. The two-dimensional calculations used one-dimensional input,
obtained from a highly successful earlier effort to model smooth pipe flow.
The one-dimensional input closely matched the smooth tube calibration performed
prior to the ribbed pipe experiment. Computational flow patterns and pressure
waveforms were compared to pictures of holographs of the experimental flow and
also to pressure waveforms obtained from the various gauges. Individual shocks
and vortices could be matched very well, as well as the pressure waveforms.

CONTENTS

ILLUSTRATIONS

TABLES

I. INTRODUCTION

Science Applications, Inc.(SAI), conducted several shock tube experiments from November 1977 to April 1978 under Defense Nuclear Agency (DNA) contract, using the shock tube facilities located at the National Aeronautical and Space Administration (NASA) AMES Research Center in Sunnyvale, California.

The smooth shock tube (Figure 1) had a driving section which was filled with high pressure helium, separated from the driven section by a metal diaphragm. The driving section was a metal cylinder 1.36 m long which tapered to a square outlet at the diaphragm. A voltage differential was introduced across a fine helical wire in the driver. This caused an explosive discharge in the helium in the driver, expelling the helium into the driven section. The shock tube itself (the driven section) was a 10-m-long, 0.1-m-diameter steel tube, which evacuated into a large steel sphere. Two of the smooth tube experiments (Run 7 and Run 10) were calculated at the Air Force Weapons Laboratory (AFWL/NTESB). These calculations were used as input to the two-dimensional ribbed tube calculations which are the subject of this report.
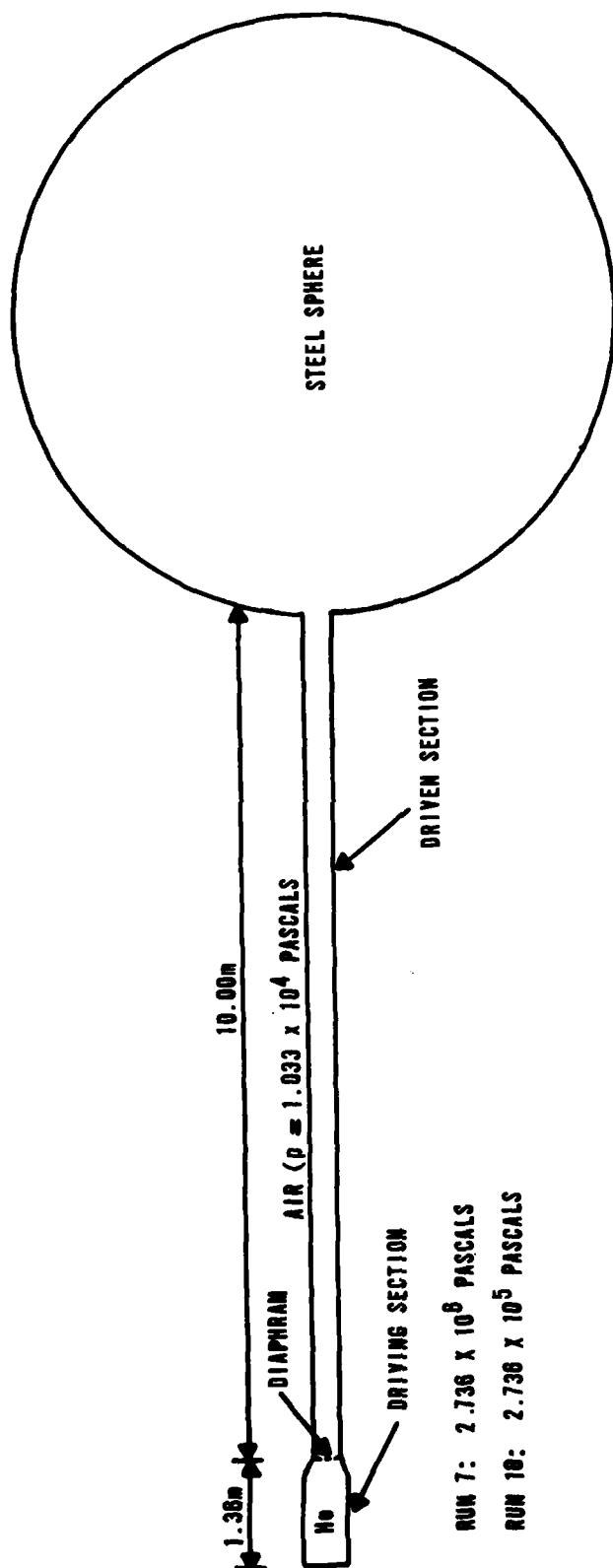
STEEL SPHERE

DRIVEN SECTION

10.00m

AIR ($\rho = 1.033 \times 10^4$ PASCALS)

DIAPHRAM

DRIVING SECTION

He

1.38m

RUN 7: 2.738×10^8 PASCALS

RUN 18: 2.738×10^5 PASCALS

Figure 1. Smooth shock tube (not to scale).

II. THE EXPERIMENTS

There were two phases to the experiments: smooth tube calibration and ribbed tube experiments. Shock tube apparatus was calibrated in the first phase using smooth shock tubes. Data from the calibration shots were obtained from pressure gauges flush with the wall of the shock tube. The performance and response of smooth shock tubes has been explored in depth, so this calibration provided an accurate experimental base on which to start.

Phase two used phase one driver conditions, so that a comparison between the control (Phase I) and the experiment (Phase II) might be made.

The experiments, calculated by AFWL, were the SAI runs numbered 7 and 10. Both runs had air pressures of one-tenth ambient (1.033×10^4 Pa) in the driven section. In the driver section, Run 7 helium pressure was 2.7×10^6 Pa, and Run 10 helium pressure was 2.7×10^5 Pa.

Arrival times from the gauges in Runs 7 and 10 smooth tube were taken by SAI and given to AFWL (Table 1). The data points were fit by a semiempirical, heuristic search computer code known as HASTUR, developed at AFWL by Murphy (1971). The resultant fit had the form:

$$D(t)_7 = 3.24517 \times 10^8 \, t^{-4} + 5.27054 \times 10^{-6} \, t^{3/2} + 3.6234 \times 10^{-2} \, t^{3/4} \text{ m} \quad (1)$$

for Run 7, and

$$D(t)_{10} = 8.96529 \times 10^{-2} \, t^{1/2} + 2.02894 \times 10^{-4} t \ln(t) \text{ m} \quad (2)$$

for Run 10.

The instantaneous slope was found for both Equations 1 and 2 by

$$\text{velocity} = \frac{dD(t)}{dt} = v(t) \text{ m/}\mu\text{s}$$

TABLE 1. SMOOTH SHOCK TUBE ARRIVAL TIMES

Run 7 Arrival Time (μs)	Station Distance (m)	Run 10 Arrival Time (μs)
235	C/2.30	392
420	D/3.42	755
627	E/4.62	1139.
820	0/5.68	no data
1001	F/6.62	1818
1245	G/7.82	2256
1513	H/9.10	2733
1774	I/10.30	3210

The two resulting equations had the form (4)

$$v(t)_7 = D'(t)_7 = 1.2981 \times 10^9 \, t^3 + 7.9058 \times 10^6 \, t^{1/2}$$

$$+ 2.7176 \times 10^2 \, t^{1/4} \text{ m/μs}$$

for Run 7, and

$$v(t)_{10} = D'(t)_{10} = 4.4826 \times 10^2 \, t^{1/2} + 2.02894 \times 10^4 \, (\ln(t) + 1) \text{ m/μs}$$

for Run 10. (5)

If one now rearranges the Rankine-Hugoniot expression for the velocity of a shock front

$$v = c \left(1 + \frac{\gamma + 1}{2\gamma} \cdot \frac{\Delta p}{P} \right)^{1/2} \text{ m/μs} \tag{6}$$

as

$$\Delta p = \left(\frac{v^2}{c^2} - 1 \right) \cdot \frac{2\gamma \, P}{\gamma + 1} \text{ (PA)} \tag{7}$$

the overpressure of the shock may be found as a function of time by substituting Equations 4 and 5 into Equation 7. Note that P = ambient pressure, Δp = over-pressure, v = velocity of the shock front, c = local sound speed, and $\gamma = c_p/c_v$ = the ratio of the specific heat of air at constant pressure to the specific heat of air at constant volume.

The arrival times were used with Equations 4 and 5 to find the velocity of the shock front. Overpressure was then plotted as a function of distance (Figures 2 and 3). Two different but constant γ's were used for each figure. The fit velocities indicated that the shock did not increase in pressure with distance (as suggested by the pressure data). These plots were compared against AFWL's one-dimensional computer calculations, described later in this report.

The ribbed shock tube was the same piece of equipment as the smooth shock tube with one section of smooth tube replaced by a ribbed section. The ribs started at a point 3.92 m from the diaphragm and ran to 6.33 m from the diaphragm, resulting in a subsection 2.41 m long. There were 64 ribs, each 3.9×10^{-3} m high and 1.57×10^{-2} m long. Spacing between ribs was 2.34×10^{-2} m.

Gauges were located in the space between ribs, flush with the top of the ribs so that the gauge would not add to the disturbance of the flow. Gauge locations for the ribbed and smooth sections are contained in Table 2.

TABLE 2. GAUGE LOCATIONS

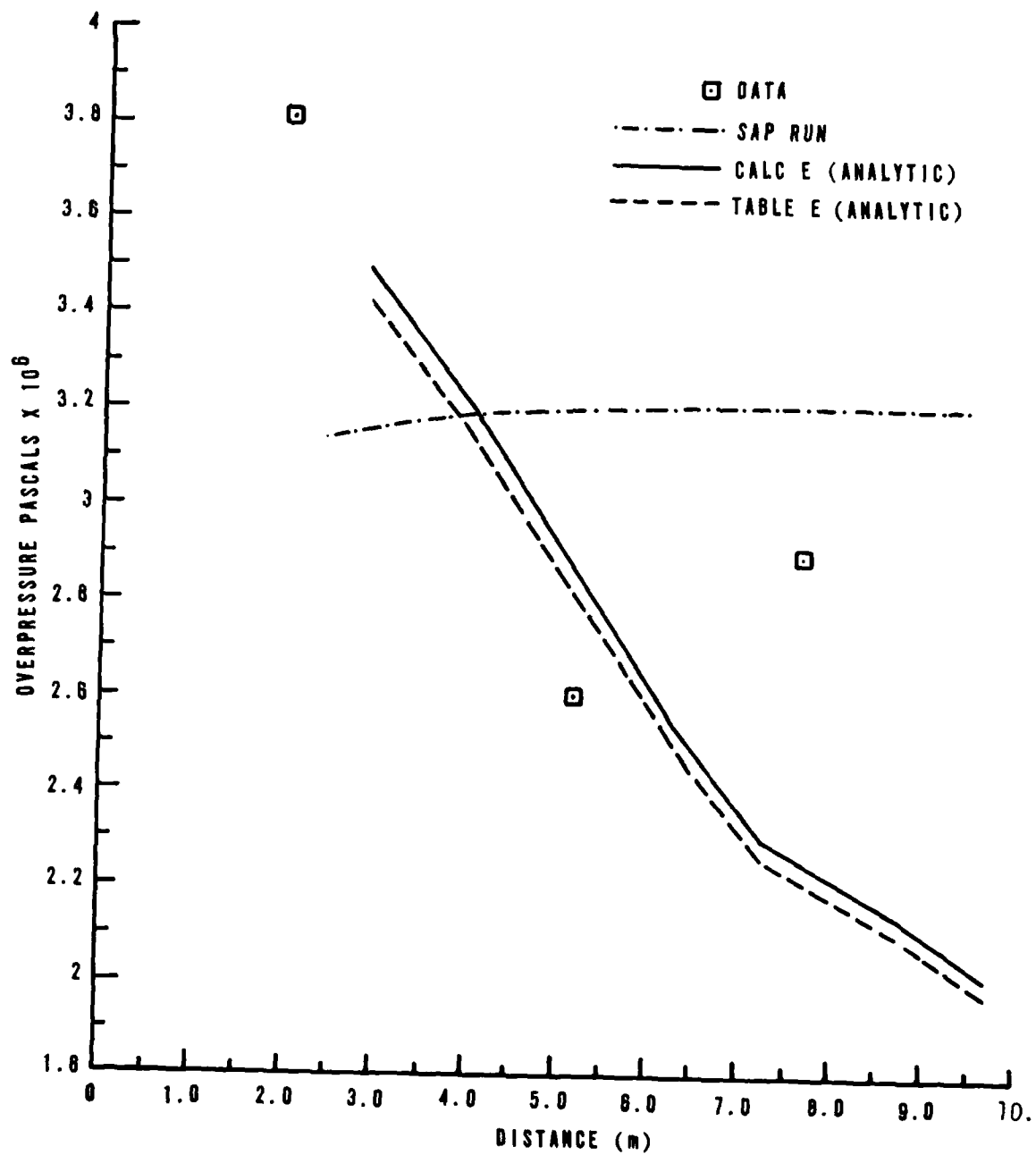| Gauge	Tube	Location (M)
C	Both	0.87
D	Both	2.01
E	Both	3.20
F	Ribbed	3.88
0, R1	Both	4.24
R, R2	Both	5.18
R3	Ribbed	6.12
G	Smooth	6.38
S'	Ribbed	6.74
H'	Ribbed	7.58
H	Smooth	7.66
I'	Ribbed	8.80
I	Smooth	8.88

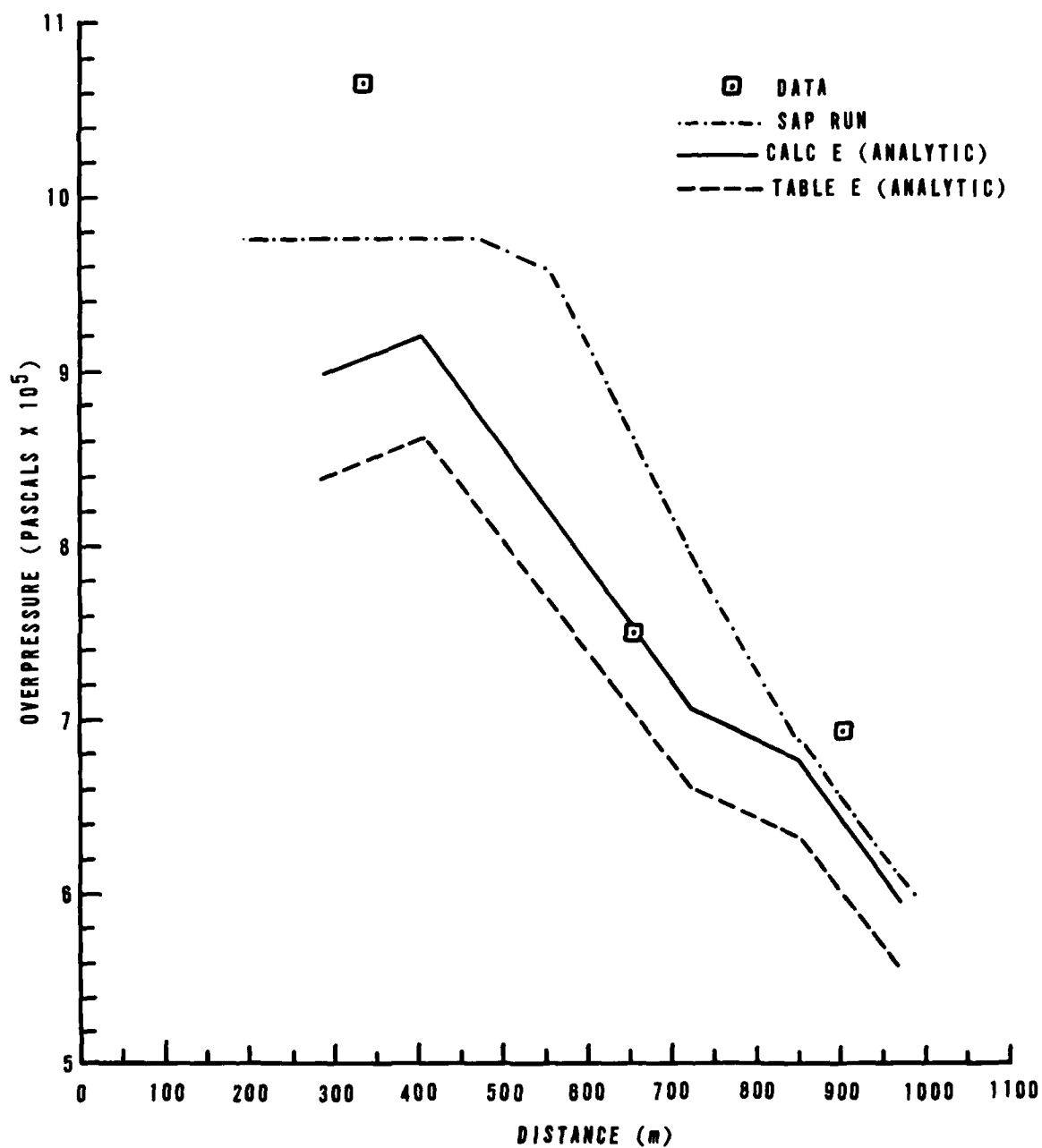Figure 2.   Run 7:   Pressure vs. distance.

Figure 3. Run 10: Pressure vs. distance.

III. THE CALCULATIONS

ONE-DIMENSIONAL SAP CALCULATIONS

One-dimensional hydrodynamic calculations were made to model the SAI smooth shock tube experiments. The one-dimensional (1-D) calculations of the waveforms and peak pressures were than used as input to the two-dimensional (2-D) hydro-dynamic calculation, which modeled the SAI ribbed shock tube experiment. The 1-D calculations were performed by SAP (Spherical Air Puff), a 1-D finite difference hydrodynamic code developed by AFWL. SAP is fully described in Reference 1.

For this problem, SAP used a Langrangian mesh. Initial zone size was 0.004 m in length. The first 36 zones (1.36 m) were used for the driver section (helium) and the next 266 zones (9.04 m) were used for the driven section (air). Total length of the mesh was 10.40 m.

In addition to the usual parameter dumps on tape, information from the hydro calculations was kept at fixed point locations, called stations. The stations kept a time history of the velocity, density and overpressure at that point. This enabled one to reconstruct a time history of the waveform of the shock at that location. Station locations were made to match experimental gauge locations for both the smooth and ribbed pipes. Additional stations were included at other locations in the mesh so that the waveform might be further investigated.

Initial conditions for the 1-D runs closely simulated the actual input conditions of the SAI experiments. Two materials were used for the calculations, and equations of state for the two materials were chosen. For air, an equation of state for real air was used (Ref. 2). For the helium equation of state, a small subroutine was used which returned

$$P = 2/3 \, \rho I \tag{8}$$

where ρ = density, I = energy density and P = pressure.

---

1. Whitaker, W. A., et al., Theoretical Calculations of the Phenomenology of HE Detonations, AFWL-TR-66-141, Air Force Weapons Laboratory, Kirtland AFB, NM., November 1966.

2. Doan, L. R. and Nickel, G. H., A Subroutine for Equation of State of Air, AFWL-TM-RTD (WLR-TN-63-2), Air Force Weapons Laboratory, Kirtland AFB, NM., May 1963.

Because the energy was restricted to temperatures well below the first ionization level of helium (about 1 eV), this equation of state sufficed.

Some controversy existed about the energy density which would be used as input for the calculation. The energy densities obtained from SAI were from a tabulated source; that is, they were readings from gauges on the capacitor bank. A calculation of the theoretical energy using

$$E = 1/2 \ CV^2 \tag{9}$$

where C = capacitance, V = voltage differential, and E = energy,

showed a difference of up to 60 percent between the calculated energy density and the tabulated energy density, shown in Table 3, received from SAI.

TABLE 3. ENERGY DIFFERENCES

Run	Tabulated I (J/kg)	Calculated I (J/kg)	Difference
7	2.014×10^7	8.7669×10^6	56%
10	2.9679×10^7	1.1974×10^7	60%

It was then decided to try four computer runs: two runs for Run 7 and two runs for Run 10, using the different energy densities and comparing the results with data. Table 4 contains the input information used for these four runs.

TABLE 4. INPUT FOR FIRST 1-D RUNS

Run	I (J/kg)	P_1 (Pa)	P_2 (Pa)
7C	8.7669×10^6	2.735×10^6	1.013×10^4
7T	2.0104×10^7	2.736×10^6	1.013×10^4
10C	1.1974×10^7	2.736×10^5	1.013×10^4
10T	2.9679×10^7	2.736×10^5	1.013×10^4

C - calculated I

T - tabulated I

The 1-D calculations took an average of 300 CDC Cyber 176 CP seconds to run to completion. The peak pressures from the stations were then plotted as a function of distance. The resulting plots (Figures 4 and 5) showed how the values of peak pressure differed from the experimental value.

It was decided to weight the energy density from Run 7 so that the difference between the two pressure versus distance curves (from the tabulated and calculated I) would converge to the experimental pressure data. Referring to Figure 4, a linear weighting formula was used:

$$E_L + \left(\frac{P_F - P_L}{P_u - P_L}\right)\left(E_u - E_L\right) = E_f \tag{10}$$

where P_F = fitted pressure, P_L = lower pressure (tabulated), P_u = upper pressure (calculated), E_u = upper energy, E_L = lower energy and E_f = fitted energy. E_f resulted in I = 1.4014 x 10^7 J/kg. Run 7 was then calculated again using this new energy density. Results of this calculation are shown in Figure 2.

The Run 10 pressure versus distance data were found to follow closely those obtained using the calculated energy density; therefore, no interpolation was necessary.

Peak pressure versus distance was then plotted for both Runs 7 and 10. The initial peak pressures were found to match experimental data, but the pressure did not drop off as rapidly in the calculation of Run 10 as did the data. Therefore, it was decided to keep the energy densities the same (so the initial peak pressure would stay the same) and shorten the driver length in the calculation, which would reduce the total energy and mass of the driver. This would cause the peak pressure to fall at a faster rate. Two runs were then made for Run 10: one with a driver length one-half and another run with a driver length one-third of the original size. By weighting the drop-off rates of the runs with the different driver lengths, a driver length of 79 percent of the original driver length was decided to match the data most closely. Another 1-D calculation was made using this driver length and was found to agree with the experimental data (Figure 3).

The 21 percent reduction in driver length is necessitated by restriction of the flow by the diaphragm support mechanism. This phenomenon was discussed with and confirmed by Dr. Dannenberg, Director of the NASA/AMES shock tube facility.
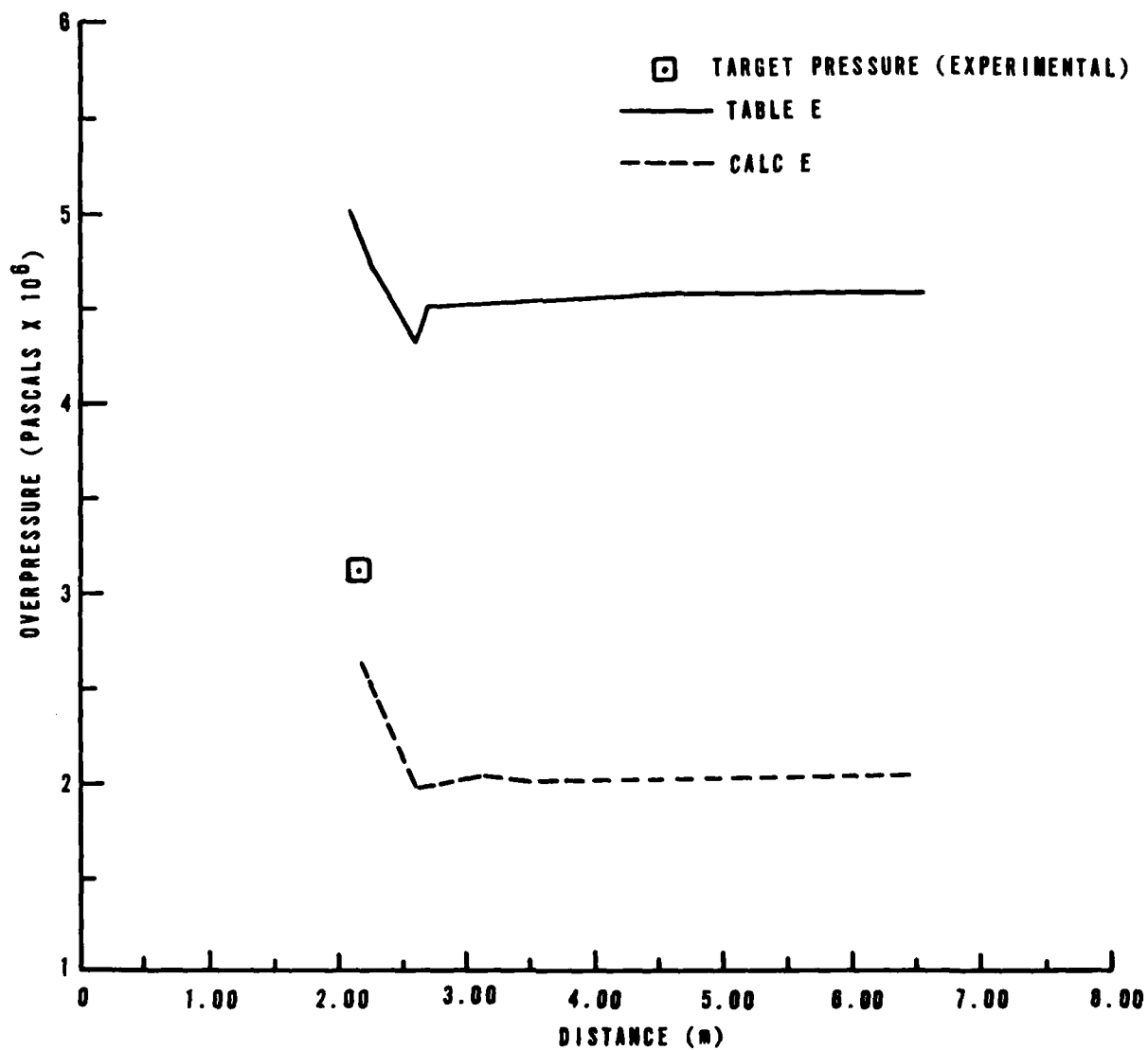
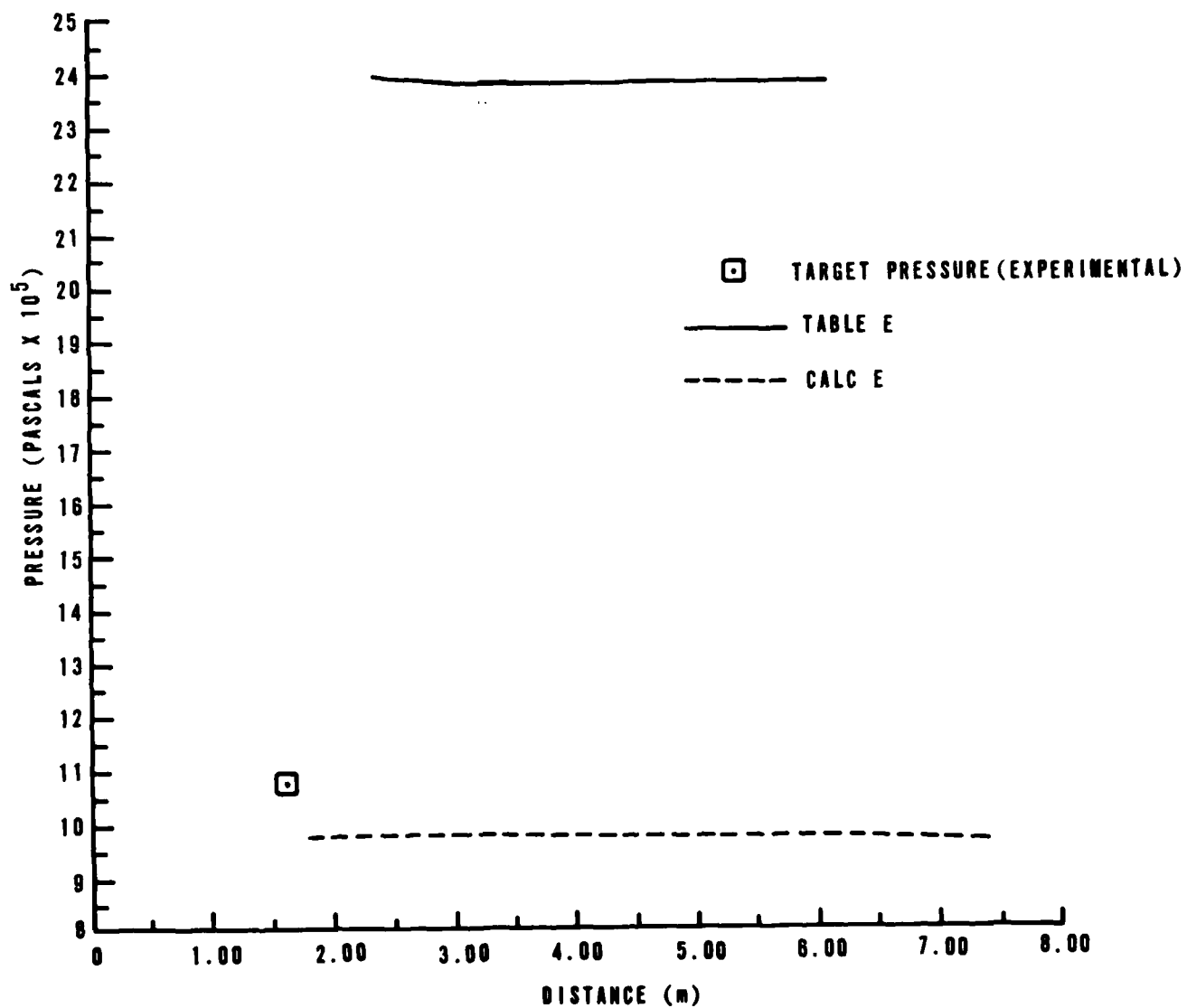Figure 4. Run 7: Initial SAP calculations.

13

Figure 5. Run 10: Initial SAP calculations.

The driver length for the Run 7 calculation was not shortened. The reasoning was that the driver pressure for Run 7 was an order of magnitude greater than that of Run 10, and subsequently the pressure waveform of the shock propagating down the tube in Run 7 would not decay as did Run 10's waveform.

Figure 6 is a drawing of a polaroid of the experimental pressure waveforms from Run 7 and Run 10. Note the decay of the waveform in Run 10 as compared with Run 7, thus verifying the assumption of no appreciable decay.

Table 5 lists the final input conditions for Runs 7 and 10.

TABLE 5. FINAL INPUT FOR 1-D CALIBRATION RUNS

Run	I(J/kg)	Density(kg/m³)	Driver Length(m)	P(Pa)
7	1.4014×10^7	0.293	34 zones = 1.36	2.736×10^6
10	1.974×10^7	0.0208	27 zones = 1.08	2.736×10^5

TWO DIMENSIONAL HULL CALCULATIONS

The one-dimensional calculations described in the previous section were used as input boundary conditions for the two-dimensional calculations. The driver section for the one- and two-dimensional calculations was the same. Because the ribs did not start until 3.92 m from the diaphragm, it was possible to take advantage of the completed 1-D calculations and use them as boundary conditions for the 2-D calculations.

The 2-D calculations were made with HULL, an AFWL-developed finite difference code. HULL was created in 1971 by Durrett and Matuska and had evolved through over 100 different versions by 1978. HULL is a dynamic,* multidimensional, Eulerian system of hydrocodes which uses the momentum, mass, and energy conservation equations with the equation of state to model hydrodynamic phenomena. The HULL differencing scheme is fully second order accurate in both time and space.** The differencing equations and complete HULL system are described in Reference 3.

---

3. Fry, M. A. et al., The HULL Hydrodynamics Computer Code, Air Force Weapons Laboratory, Kirtland AFB, NM., September 1977.

*Dynamic in the sense that HULL selects and compiles only those subroutines it needs, keeps a tape library, etc.

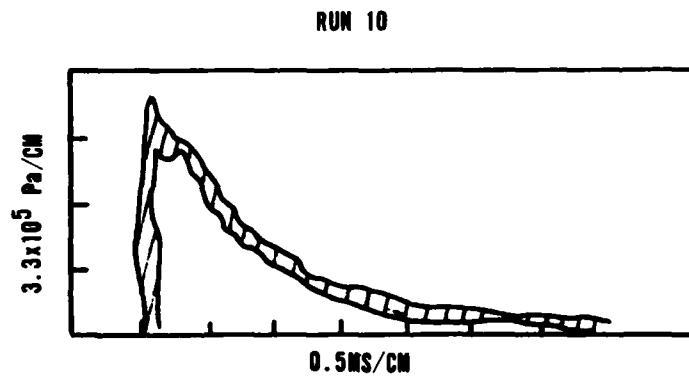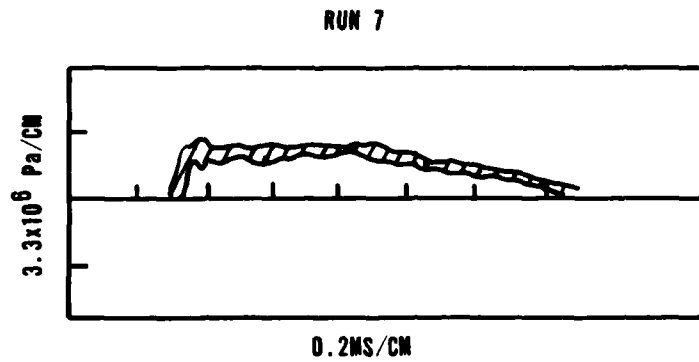**In the Lagrangian phase.

RUN 7

RUN 10

Figure 6. Run 7 and Run 10. Experimental Pressure Waveforms.

Boundary and Input Conditions. First, we must insure that any reflected or rarefacted wave generated at the rib would not propagate back to the boundary of the mesh before the shock passed through the entire length of the shock tube. If this were allowed, the reflected or rarefied wave would reach the bottom of the mesh, causing unrealistic perturbations to the flow. Second, the input shock must stabilize. Because the HULL differencing technique was different from the SAP differencing technique (Eulerian vs. Lagrangian), the hydro would be performed differently when the shock left the SAP mesh and was input in the HULL mesh.

When the preceding conditions were taken into consideration, a distance equal to seven inner diameters of the shock tube was established between the bottom of the mesh and first rib location.

Two calculations using one material (air) were made for the ribbed experiments corresponding to the smooth tube Runs 7 and 10. A third calculation was made using a very fine mesh with one material (air) for the Run 10.

Geometry I. The mesh for the first two runs was 6.8054 m long and 0.0547 m wide. The mesh modeled the shock tube, with the left hand boundary of the mesh corresponding to the axis of symmetry of the shock tube. The mesh used a constant zone size over the ribbed section, with an increasing zone width ratio of 10 percent and length ratio of 1 percent until the axis of symmetry was reached radially and the end of the shock tube was reached axially. The first 13 radial zones from the shock tube wall, moving radially towards the axis of symmetry, had a zone width of 1.3×10^{-3} m. Zone width then increased by 10 percent for the next 11 zones until a maximum zone width of 5.6×10^{-3} m was reached at the axis. The first 403 axial zones (0.5239 m), starting from the input boundary, had a length of 7.8×10^{-3} m. After the last rib, zone length then increased by 1 percent per zone for the next 151 zones (6.2815 m). until a maximum zone length of 3.5×10^{-2} m was reached at the end of the shock tube. Thus, a subgrid of unvarying zone size existed in the mesh, having zones 1.3×10^{-3} m in width by 7.8×10^{-3} m in length (Figure 7).

The ribs and trench wall were modeled by perfectly reflecting zones known as islands. The ribs were modeled as rectangles by islands 3 zones high (3.9×10^{-3}m) and 2 zones wide (1.56×10^{-2} m). Spacings of 3 zones (2.34×10^{-2} m) were used between the ribs. At the locations corresponding to SAI gauge locations, the space between the ribs were filled by islands, corresponding to the geometry in the test.
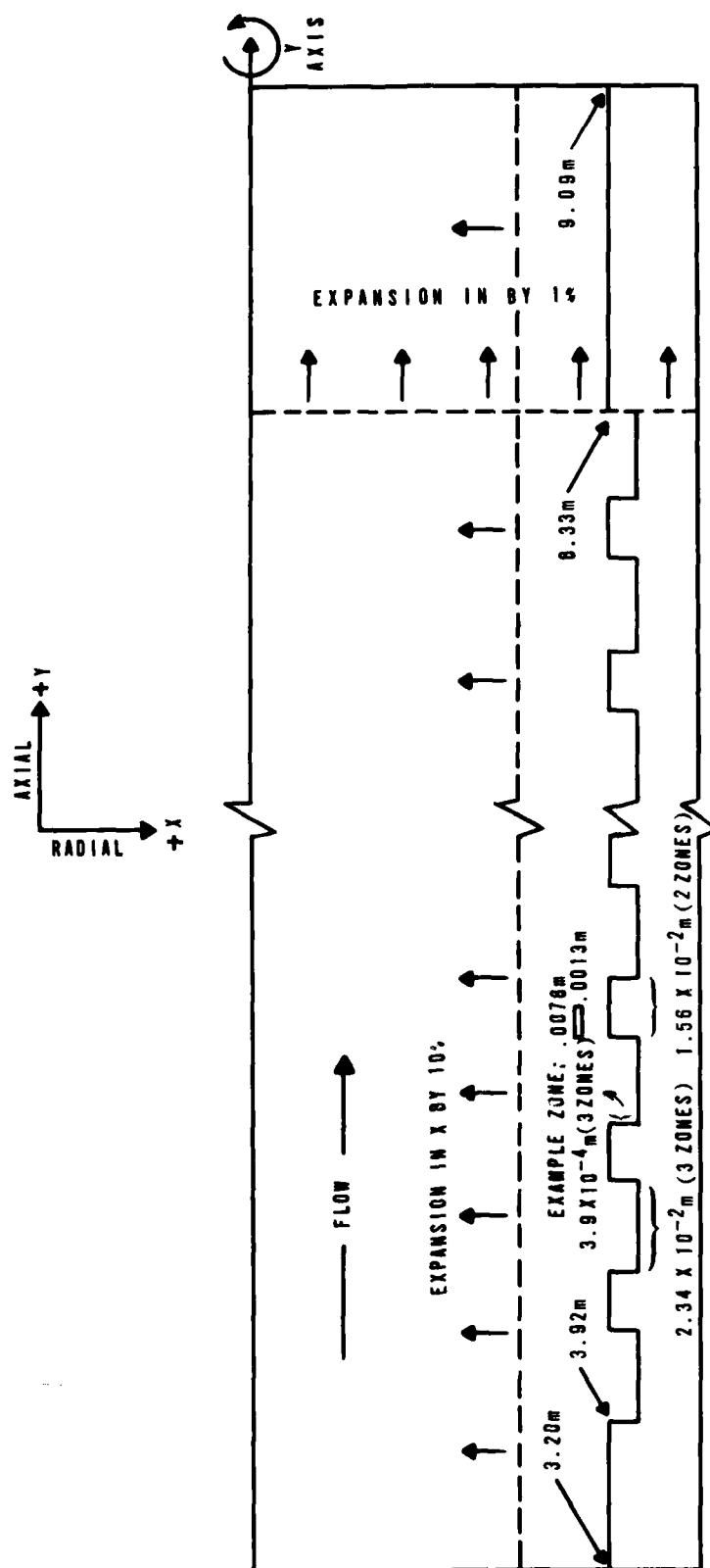
17

Figure 7. Coarse Mesh.

Stations were placed at all SAI gauge locations as well as throughout the rest of the mesh so that a time history of the flow parameters could be observed at various points of interest.

Geometry II. The fine zone calculation using Run 10 input boundary conditions used constant square zones of 6.5 x 10^{-4} m on a side throughout the entire mesh.

The mesh was 0.40590 m long (626 zones) by 0.0590 m wide (86 zones), resulting in a total of 53,836 zones. The mesh started at 3.8875 m from the diaphragm and ended at 4.29440 m (Figure 8). This left 0.0325 m (50 zones) before the ribs. A distance of seven inner diameters before the ribs was not chosen, as only nine ribs were modeled and the shock was observed to propagate through the mesh before any reflected or rarefied wave propagated upstream to that distance. Fifty zones were chosen so that the input shock from the SAP 1-D Run 10 calculation would stabilize. If a distance of seven inner diameters (0.7098 m) had been used, 93,913 additional zones would have been added, making a total of 147,778 zones. This would result in nearly a factor of 3 increases in both run time and cost, without reaping any benefits.

The ribs were modeled by islands 6 zones high (3.9 x 10^{-3} m) and 24 zones wide (1.56 x 10^{-2} m). Spacings of 36 zones (2.34 x 10^{-2} m) separated the ribs. A total of nine ribs were in the fine zone calculation, with the space between the last two ribs filled with an island to model the first gauge position.
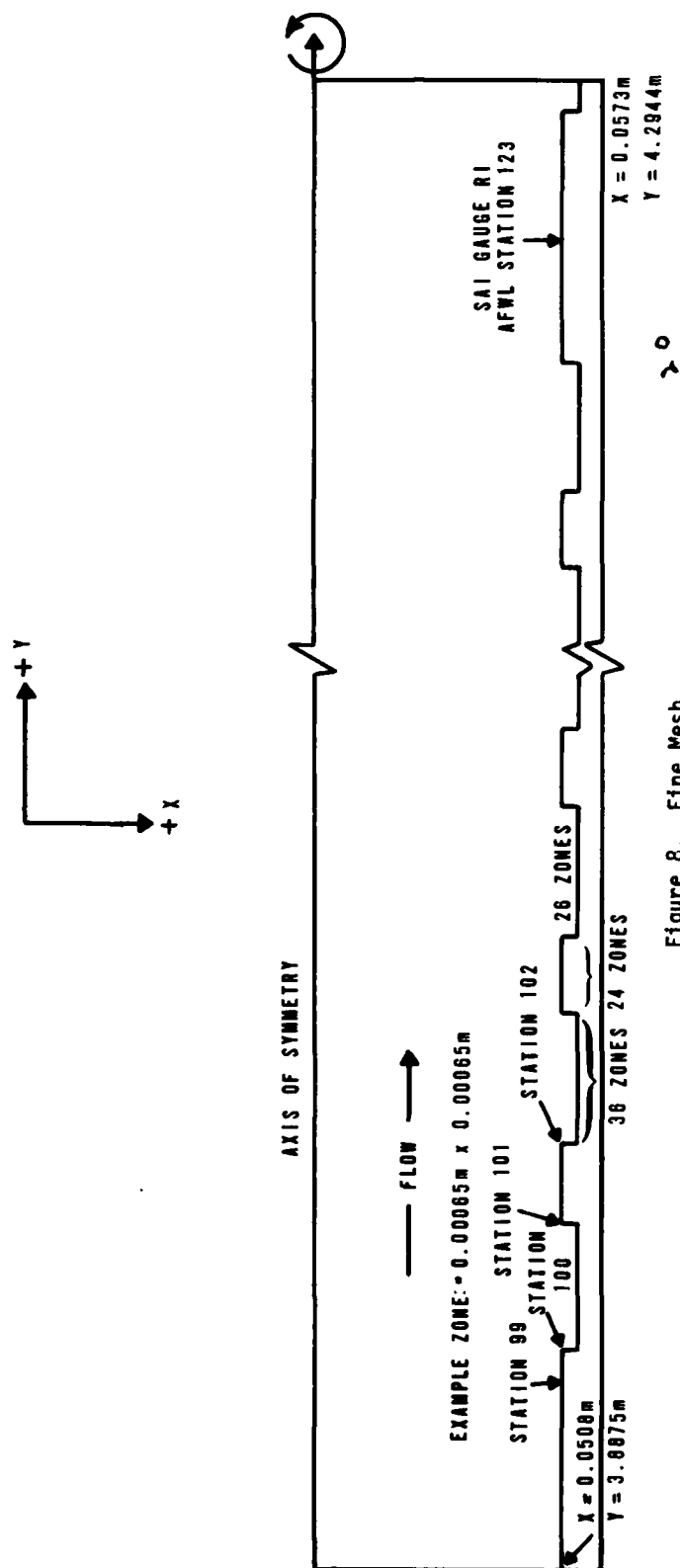
Figure 8. Fine Mesh.

IV. RIBBED SHOCK TUBE RUNS

The two ribbed shock tube calculations were run on a CDC Cyber 176. The runs took approximately 6.5 CPU hours each, averaging 5000 cycles per run. The two calculations differed only in the input conditions from the two 1-D calculations (driver pressure of 2.7 x 10^6 Pa in Run 7 versus 2.7 x 10^5 Pa in Run 10).

The shock propagated up the tube from the input boundary. The shock took approximately 15 to 20 zones to stabilize because the 1-D input was calculated with much larger zone sizes compared to the 2-D zone sizes (0.04 m in the smooth tube versus 0.0076 m in the rough tube). A stable shock soon developed in the smooth part of the tube. The shock at this time had the same rise and a similar waveform as the 1-D input shock. The arrival times of the two shocks were offset by a constant because the position of the input boundary of the 2-D calculation was slightly less than the station location of the 1-D shock that was input. As shown by Figure 9, the two-dimensional shock waveform had a faster rate of decay than the 1-D shock at this position. This was attributed to a rarefaction wave propagating upstream after the shock reached the first rib interface. This rarefaction wave tended to enhance the decay of the waveform at that point.

Referring to Figures 7 and 8, the ribs in the ribbed shock tube were actually recessed into the tube. In other words, the smooth section was broken by a series of recessions, or troughs, and the ribs are points where the troughs are flush with the shock tube wall (Figure 10).

FLOW IN THE FIRST TROUGH

When the shock reached the first trough (see Figure 11), the outer edge of the shock front (i.e., that part in contact with the shock tube wall) spilled over the edge of the trough. At that time, the shock front near the axis had no information that the shock front edge had spilled into the trough. Thus the shock front near the axis remained undisturbed. The shock front edge, however, experienced an expansion and a subsequent loss of energy as it spilled over the edge.

As the shock front advanced over the first trough, the flow behind the shock front edge continued to spill down into the trough. The shock front edge continued to propagate into the trough until it hit the corner made with the trough wall and the bottom of the trough. The impact generated a reflected shock
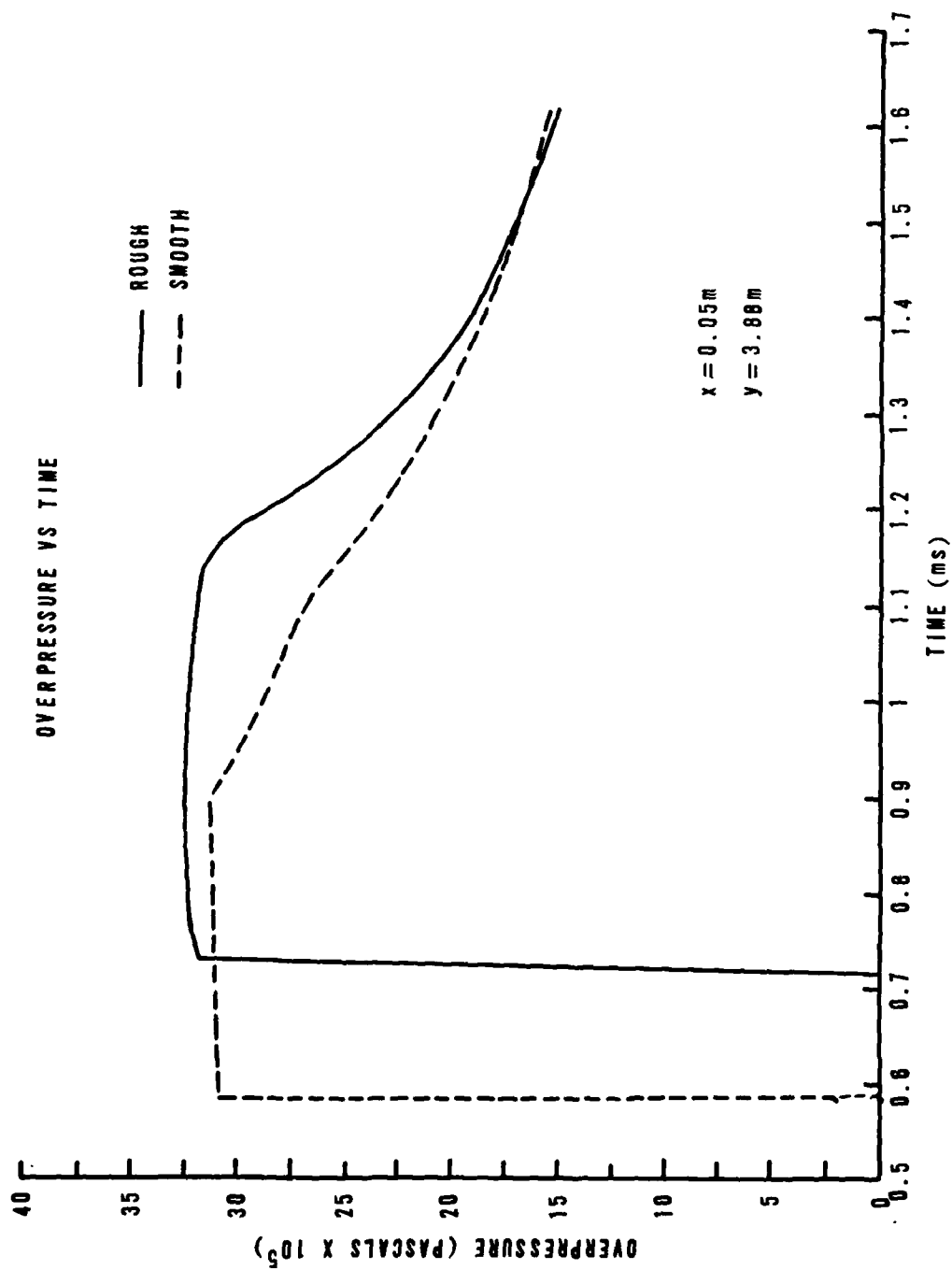
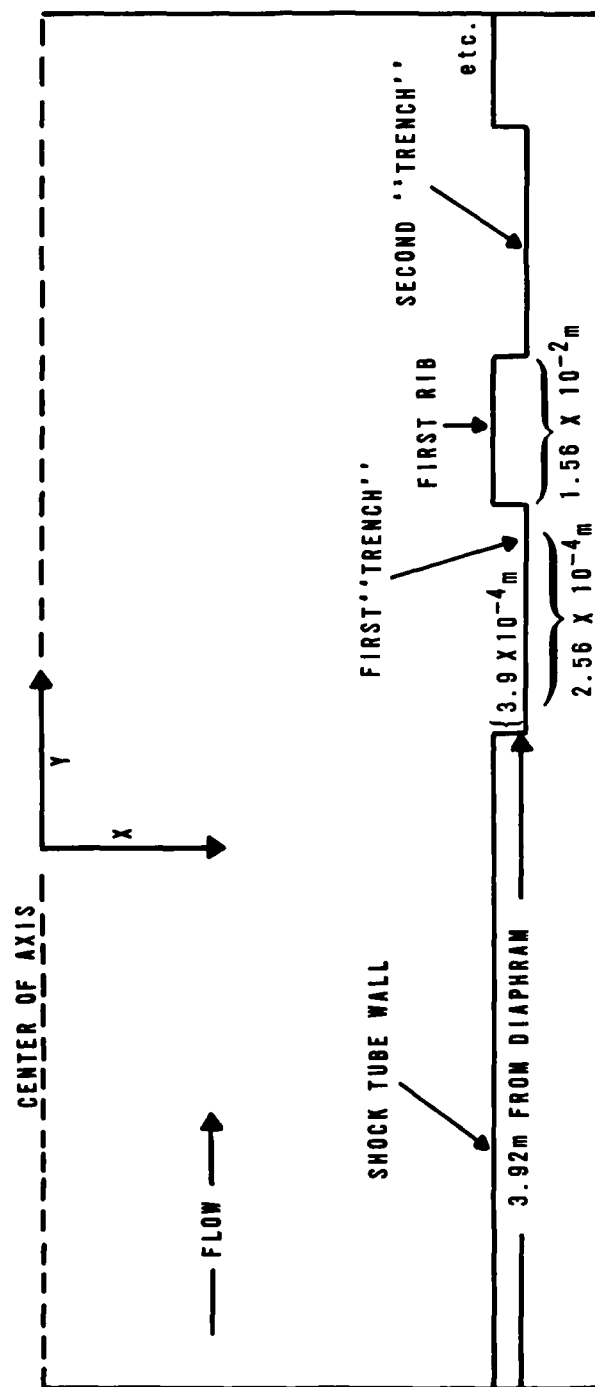Figure 9. Run 7: 1-D Input/2-D boundary.
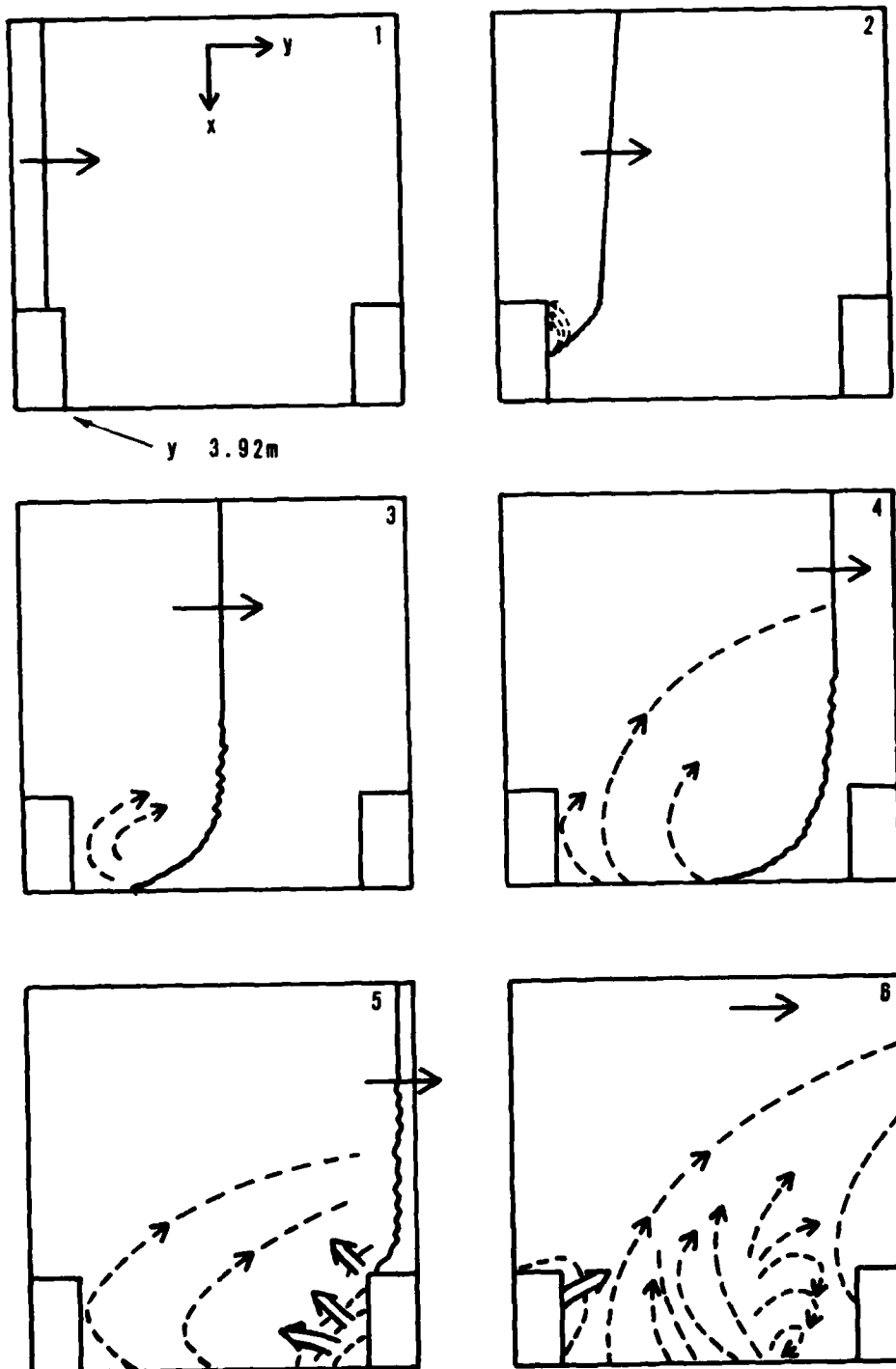
Figure 10. Trench/Rib convention.

Figure 11. Flow in the first trench.

which propagated from the trough bottom towards the opposite trough wall. The original shock front edge continued to expand into the trough. The first evidence of a curving of the entire shock front arose when the shock front edge (that was experiencing expansion) hit the bottom corner of the opposite trench wall, 0.1 µs before it hit the top of the opposite trench wall. The shock front near the center of axis continued to propagate undisturbed. The shock front at the center of axis arrived at a point above the opposite trench wall 0.2 µs before the perturbed shock reached the opposite wall of the trough.

Once the shock hit the opposite trough wall, the shock was reflected upstream. Figure 11 depicts the timing sequence of the first trough experienced.

The flow in the bottom of the trough steadily decreased, changing to a direction toward the first trench wall. By studying contour diagrams of this region, one immediately observes the vortices thus formed between the ribs (Appendix A).

When the shock reached the ribbed portion of the tube. a rarefaction and compression wave developed. The compression wave (or bow wave) propagated up the tube with the flow, while the rarefaction wave propagated back down the tube toward the input boundary. Each time a rib was hit by the shock front, a rarefaction and compression wave developed. The bow waves arched towards the middle of the shock tube (axis) and interacted with the waves developed from previous ribs. The interaction of the bow waves and shock front produced a new shock front consisting of multiple shock waves. This may be seen in density contour plots of the calculation (Figure 12). Contour plots were obtained from hydro data (velocities, pressure, mass and energy) which were stored on tape periodically during the calculation.

The ribs slowed the shock in the sense that the arrival times for the shock in the ribbed calculation were slightly greater than the arrival times for the smooth calculation. The ribs also caused the initial peak pressure to drop, followed by an increase in pressure greater than that observed in the smooth calculation (Figure 13). This increase in pressure was attributed to stagnation, i.e., the dynamic pressure was converted to overpressure. This is demonstrated in Figure 14, which compares the smooth tube dynamic pressure with the ribbed tube axial dynamic pressure at a point 5.18 m from the diaphragm. The pressure waveform does not change significantly along the radial direction.
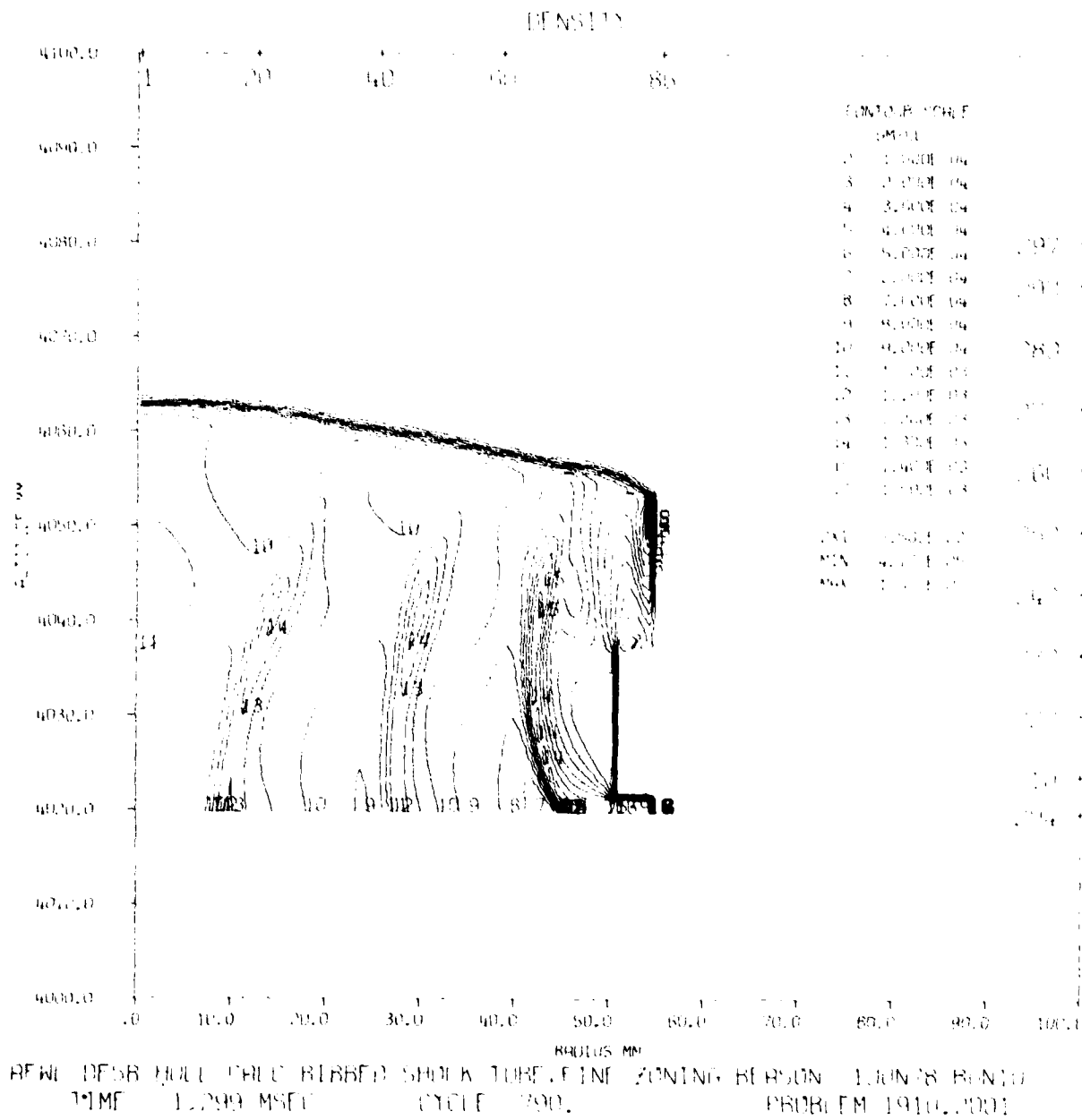
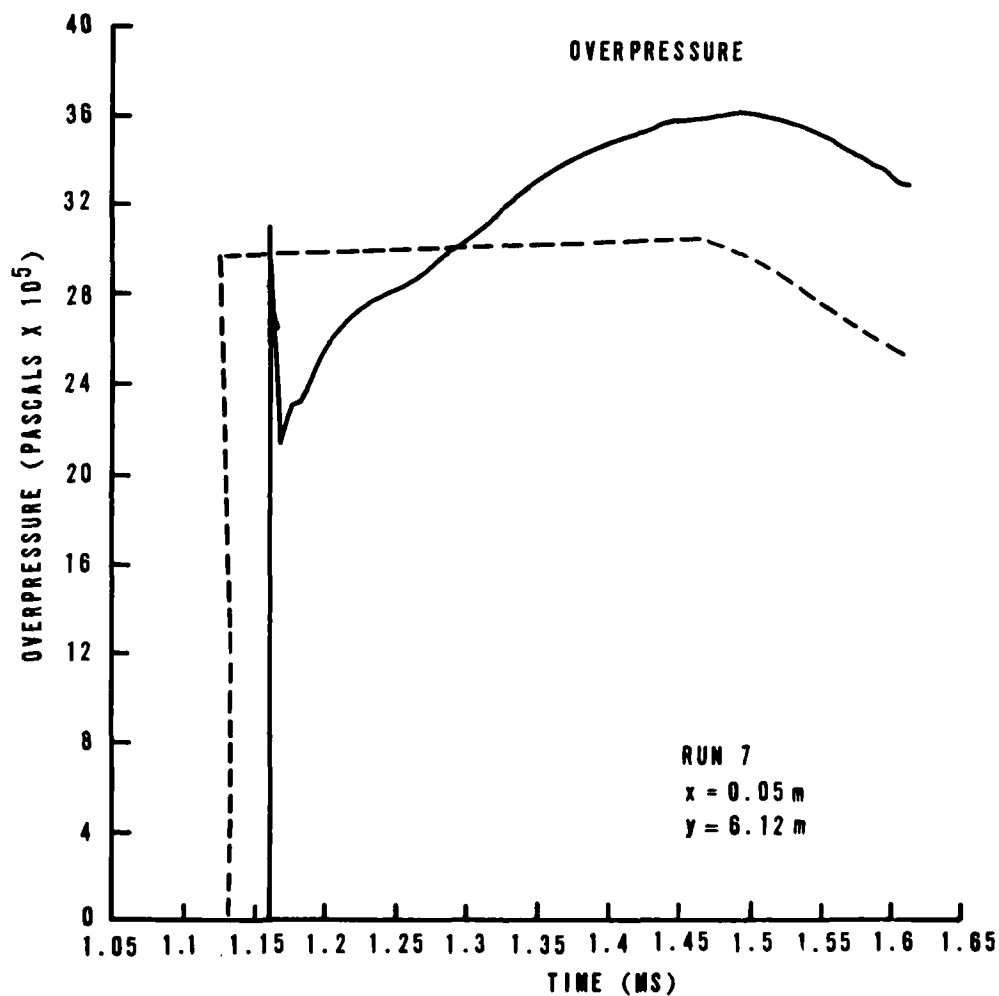Figure 12.   Computer generated density contour plot.

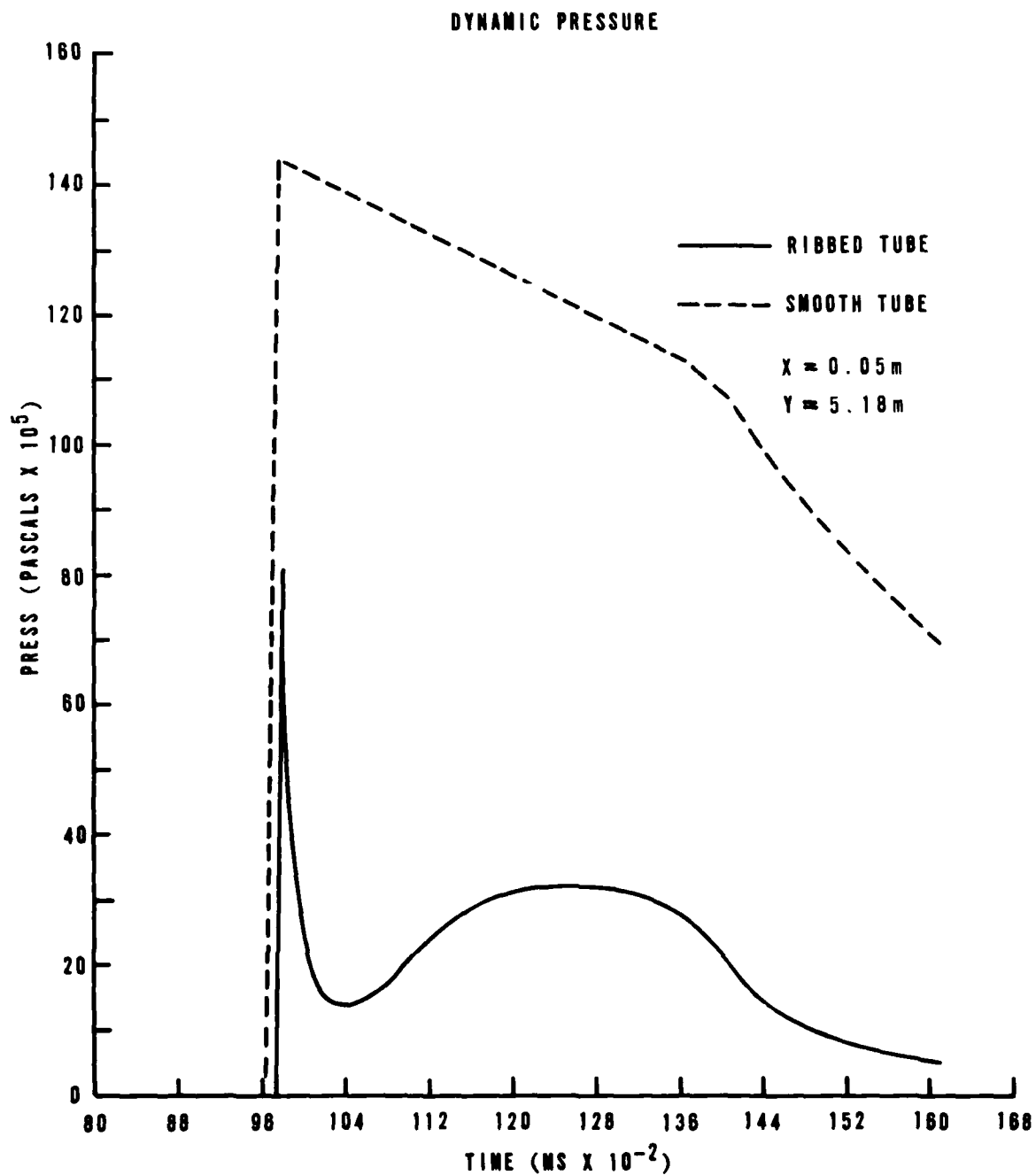Figure 13. Comparison of smooth and rough tube.

Figure 14.   Rough and smooth tube comparison.

FINE ZONE CALCULATION

Some question arose concerning the accuracy of using zone sizes of 7.6×10^{-3} m by 1.3×10^{-3} m, so a very fine zone calculation was made of Run 10. This fine zone calculation used a constant zone size of 6.5×10^{-4} m by 6.5×10^{-4} m which covered the first eight ribs.

Like the coarse zone calculation, the fine zone calculation took approximately 20 zones to stabilize the shock. Once the shock front hit the first rib, the shock wave lost strength as it flowed down the side of the rib. This resulted in a rarefaction wave propagating upstream. A bow wave was immediately formed as the shock rose over the next rib.

One may further appreciate the significance that the first protuberance (rib) had on the flow by studying the time histories of various parameters near the first rib. The following time histories all occurred at equal radial distances (5.037×10^{-2} m) from the axis, and at varius axial distances.

The time history of the overpressure 2.5×10^{-3} m before the first trench (3.9175 m) from the diaphragm, station 99) closely followed the time history of the 1-D input wave. A peak of 1.5×10^6 Pa with a sharp drop off by a factor of 3 in 0.2 ms was observed, followed by a slow decay to 0.8×10^6 Pa in a 2.2 ms. The calculation had not been run further as the initial shock had already passed through the mesh.

At the point where the first trough started (3.9023 m from the diaphragm, station 100), a time history of the overpressure showed the wave initially behaving as a 1-D shock peaking at 1.2×10^6 Pa, dropping off to 8×10^5 Pa. One-half millisecond later, however, the overpressure sharply climbed to a maximum of 1.47×10^6 Pa. The wave then fell slightly and climbed again, resulting in two peaks in a span of 0.3 ms. The overpressure then decayed (Figure 15). Station 101, 2.2×10^{-2} m downstream from station 100, kept a time history of flow parameters at the point where the first trough ended and the first rib began (Figure 8). Stagnation of the flow is readily apparent at this point. Figure 16 shows the axial dynamic pressure dropping as the overpressure at that point increases (i.e., kinetic energy converted to potential energy), indicating the stagnation due to the reflected shock coming from that rib. Thus, the second peak observed in the overpressure at station 100 (Figure 15) is attributed to the reflected shock from the first rib.
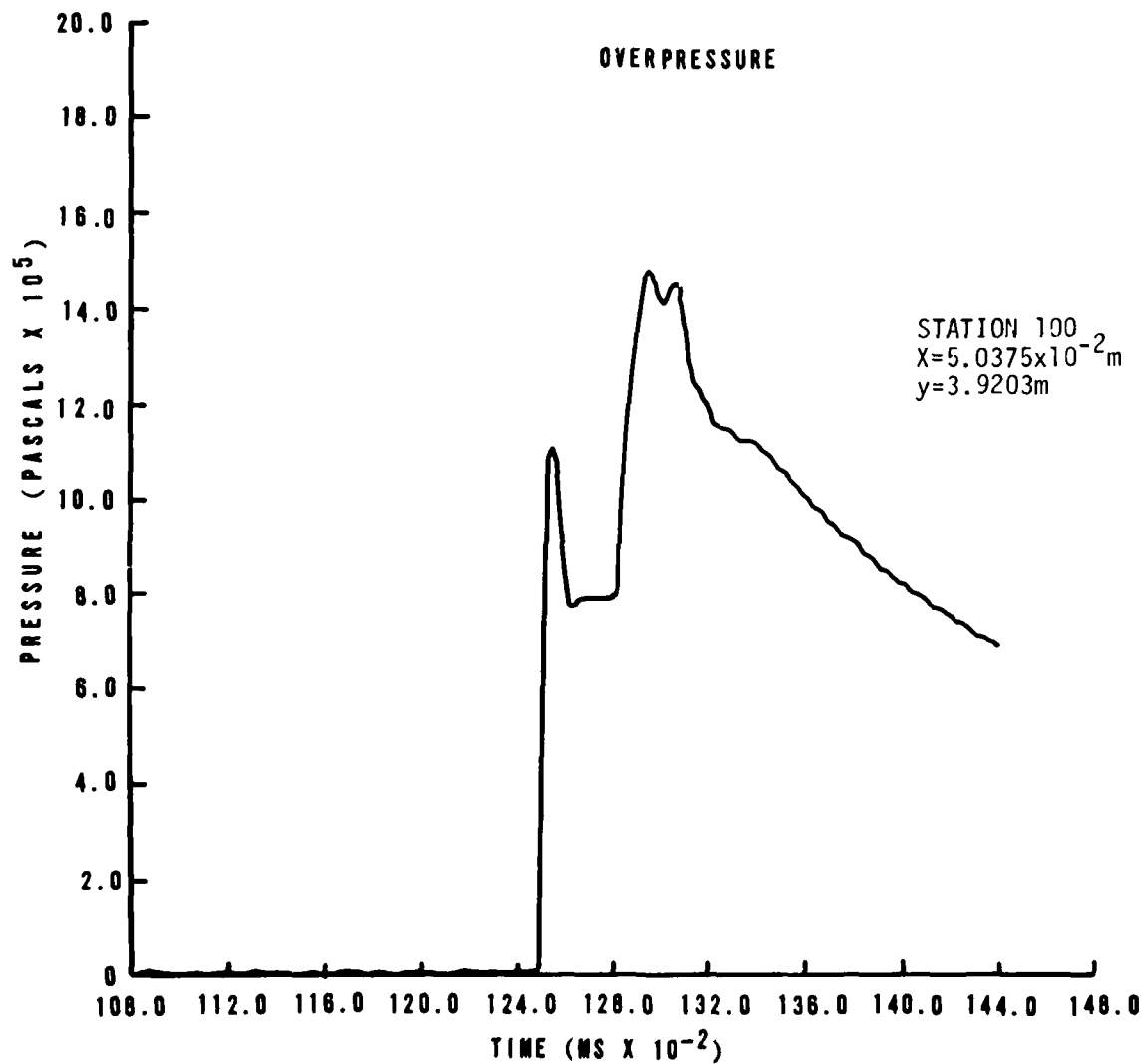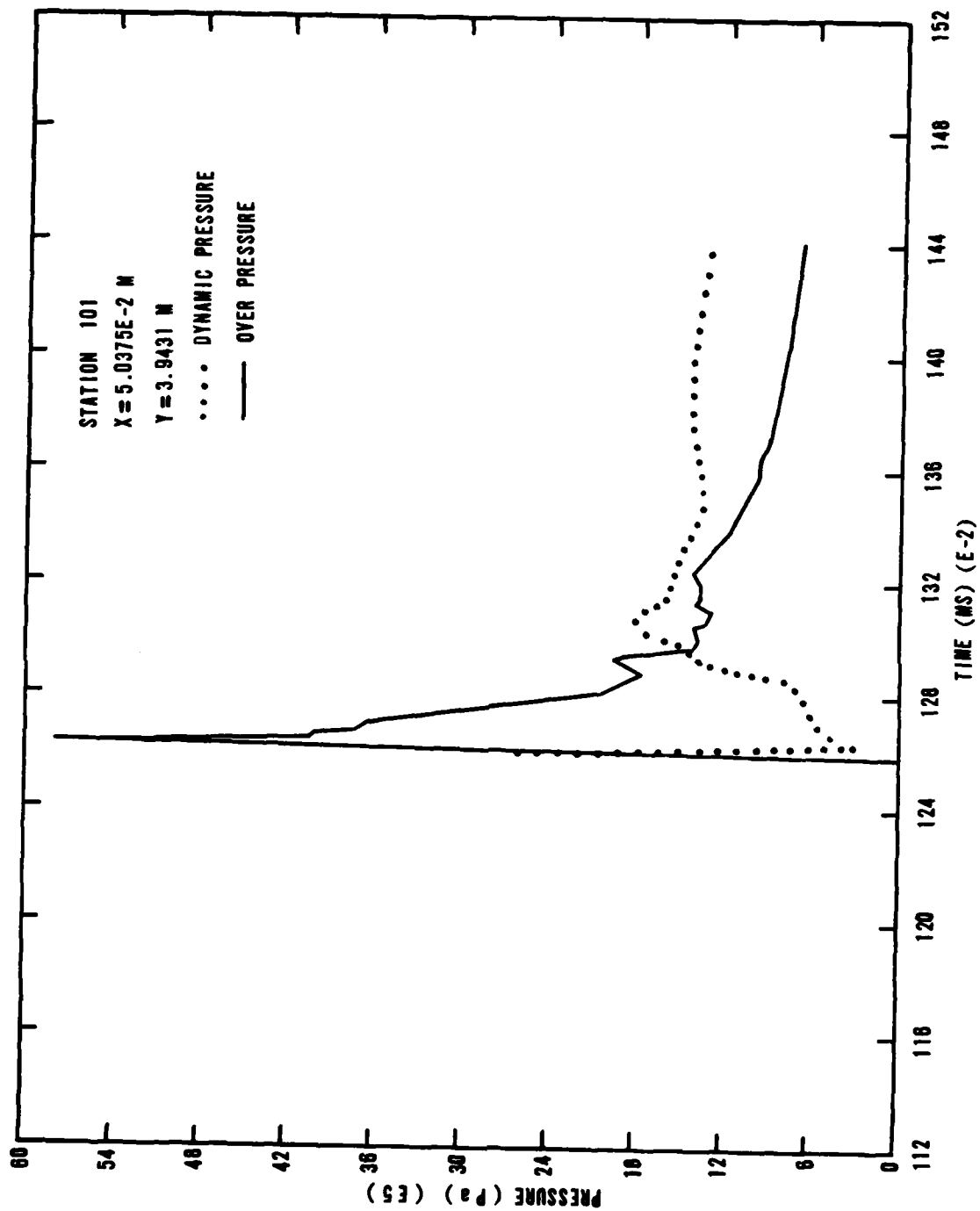
Figure 15. Station 100 overpressure, fine zone.

Figure 16. Station 101 overpressure/dynamic overpressure, fine zone.

The formation of bow waves or compression waves and rarefaction is seen when one studies density contour plots of the flow (Appendix A). A density contour plot was compared to a picture that SAI took, using holography, of a ribbed shock tube. Figure 17 shows the close similarity between the picture of the flow and the computer generated plot. One should note the equal number and position of visible bow waves, the bending of the shock front, and the location of the waves, indicating that the fine zone calculation closely matches the experiment.

Pressure waveforms from the fine zone calculations were compared with digitized experimental wave forms (Appendix B). The wave forms, peak pressures, and rise agree to an extent. The coarse zone calculation compared to within 20 percent of the fine zone calculation, indicating that the coarse zone calculation was a good run for qualitative and some quantitative purposes.

Figure 17. Picture of holograph.

V. CONCLUSIONS

The HULL hydrocode has modeled two ribbed shock tube experiments. An
extensive amount of work was accomplished to insure that the exact input
conditions (as far as pressures, energies and waveforms) were met. One-
dimensional calculations modeled the preliminary smooth shock tube experiments.
The one-dimensional calculations were adjusted to closely match unique input
conditions. These one-dimensional calculations were used as input for two-
dimensional calculations which modeled the ribbed shock tubes. A very fine zone
calculation was then run to verify the use of coarse zones. The fine zone
calculation indicated that errors were less than 20 percent between the coarse
and fine zone runs. Waveforms of the smooth and rough tube runs were compared
and found to differ, as expected. The main differences in the rough tube runs
were greater arrival times, smaller initial peak pressures, and a greater over-
pressure (attributed to stagnation).

Density contour plots of the flow were compared with a picture of a holograph
of a ribbed tube and found to match closely. The computer generated plot was
found to show the major bow waves and bending of the shock front which could be
seen in the photograph. The plot also showed the presence of a disturbance
(vortex) near the ribs after the shock passed by.

It has been shown that in both quantitative and qualitative comparisons
between experiment and computation, HULL has modeled the physical phenomena
observed in ribbed shock tubes. By using coarse zones, errors were increased
by 20 percent or less, indicating that HULL is a powerful tool in examining
this perturbed type of flow with less run time by using coarse zones instead
of very fine zones.

APPENDIX A

DENSITY CONTOUR PLOTS

Pressure, density, energy and velocities of each zone are stored on tape at standard times; i.e., times which are specified by the programmer. These thermodynamic variables are used to produce contour plots. The following density contour plots were made in several regions. The first region is the area near the first trough, the other regions were in upstream troughs.
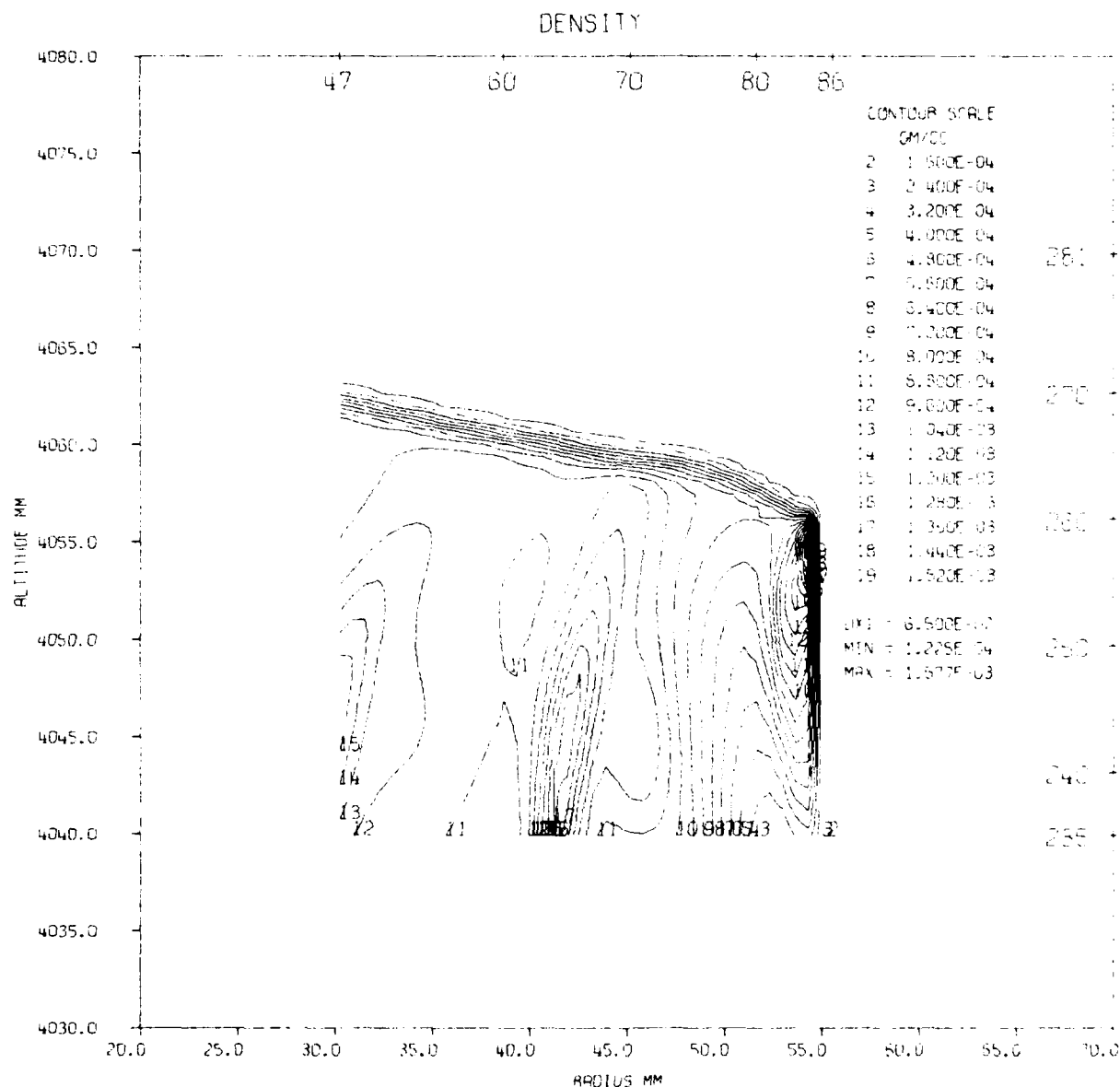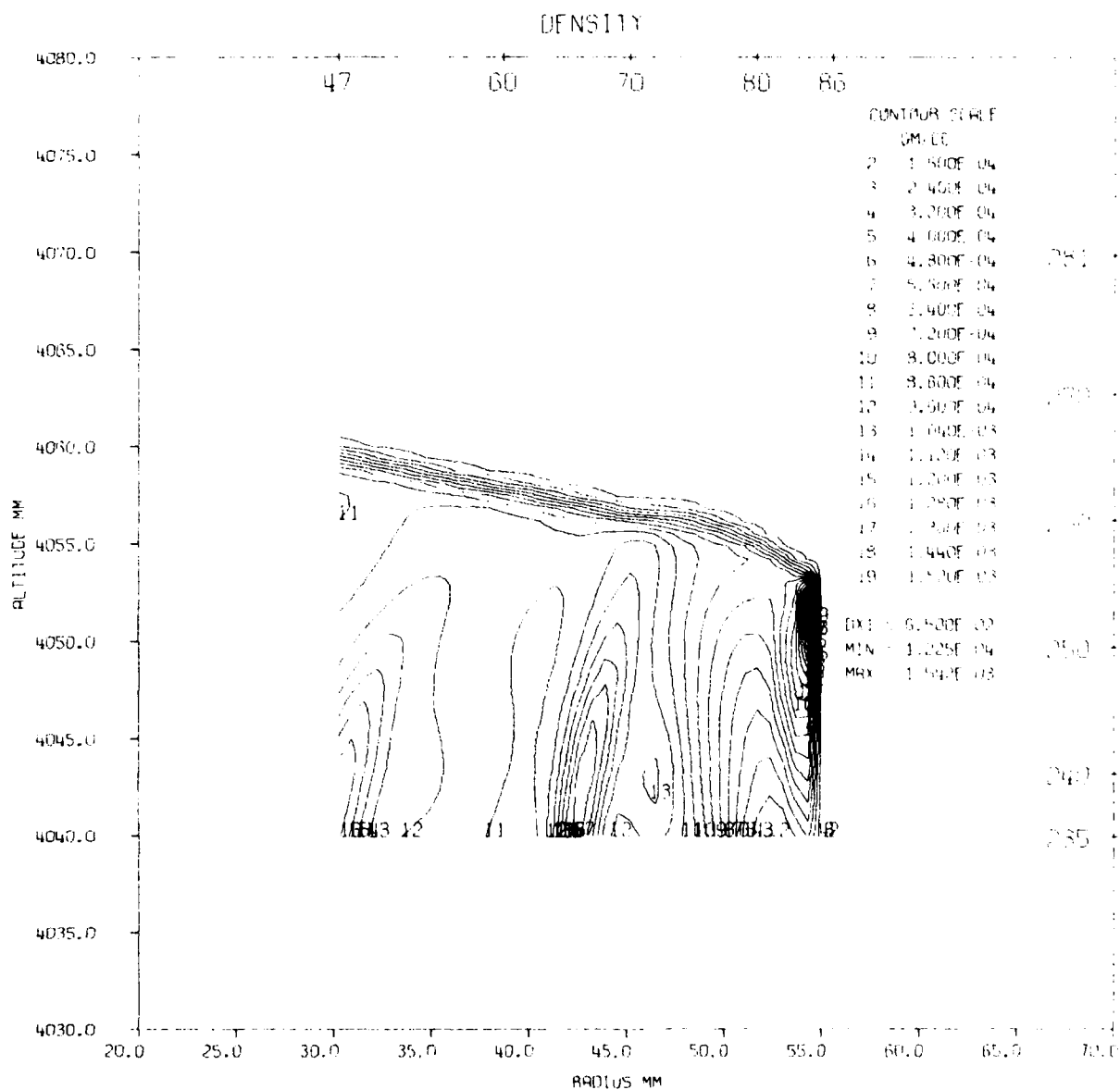
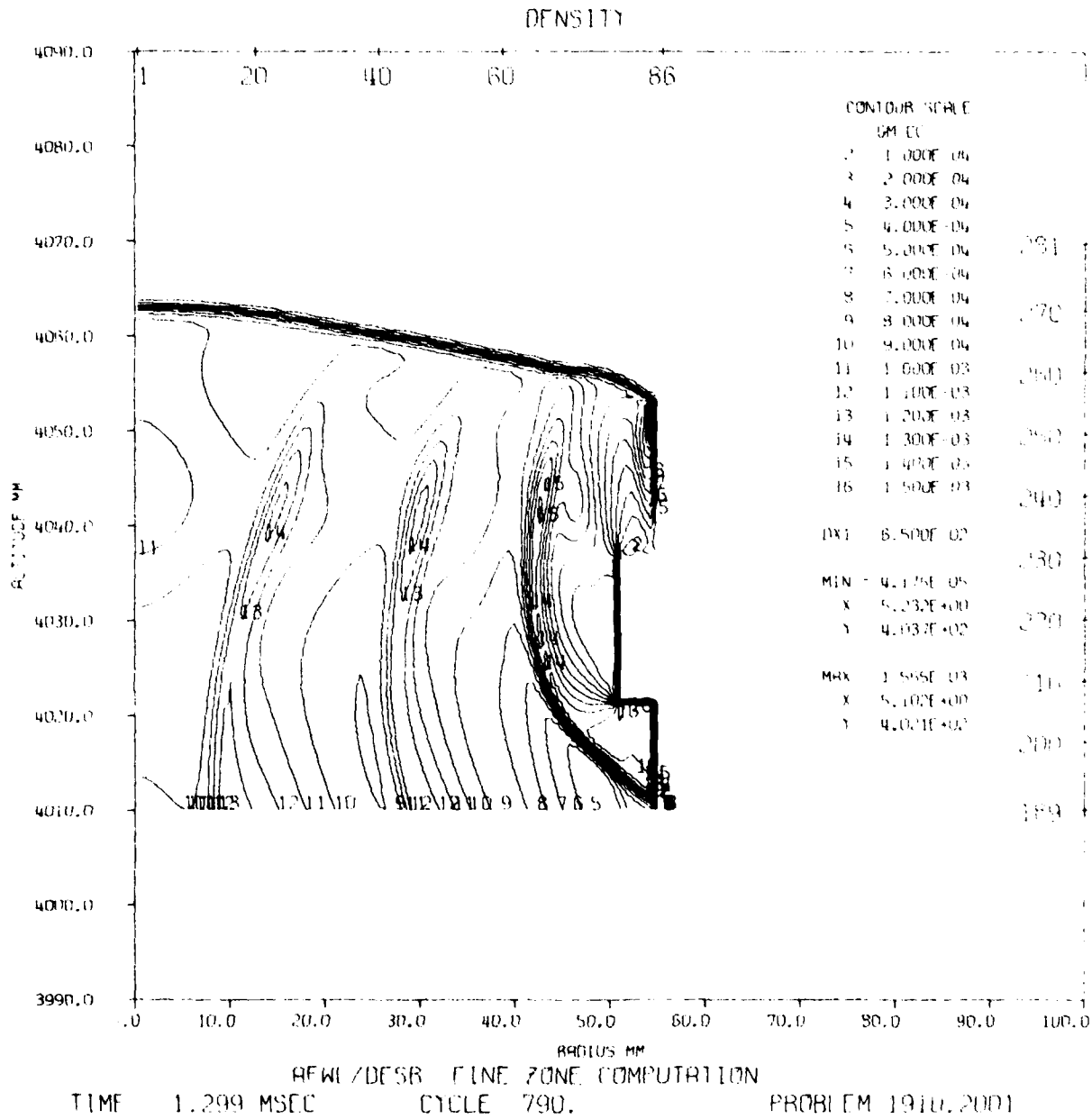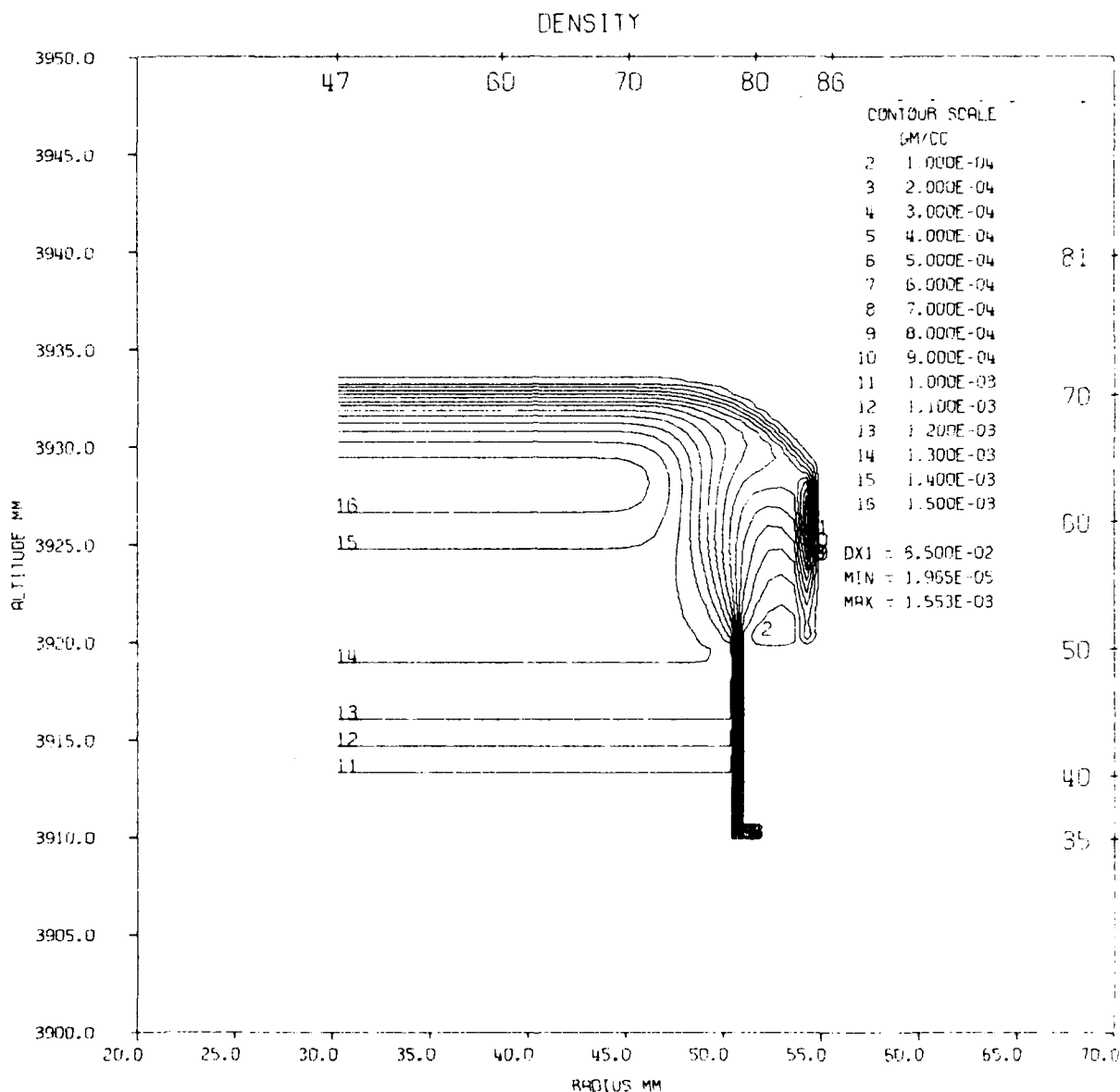DENSITY

CONTOUR SCALE
GM/CC

ALTITUDE MM

RADIUS MM

AFWL/DESB HULL CALC-RIBBED SHOCK TUBE.FINE ZONING-BERSON 1JUN78 RUN1U
TIME   1.300 MSEC   CYCLE 799.   PROBLEM 1910.2001

AFWL/DESB FINE ZONE COMPUTATION
TIME 1.300 MSEC   CYCLE 799.   PROBLEM 1910.2001

37

AFWL/DESB HULL CALC-RIBBED SHOCK TUBE, FINE ZONING-BEASON
TIME 1.300 MSEC   CYCLE 799.   PROBLEM 19110 AND

38
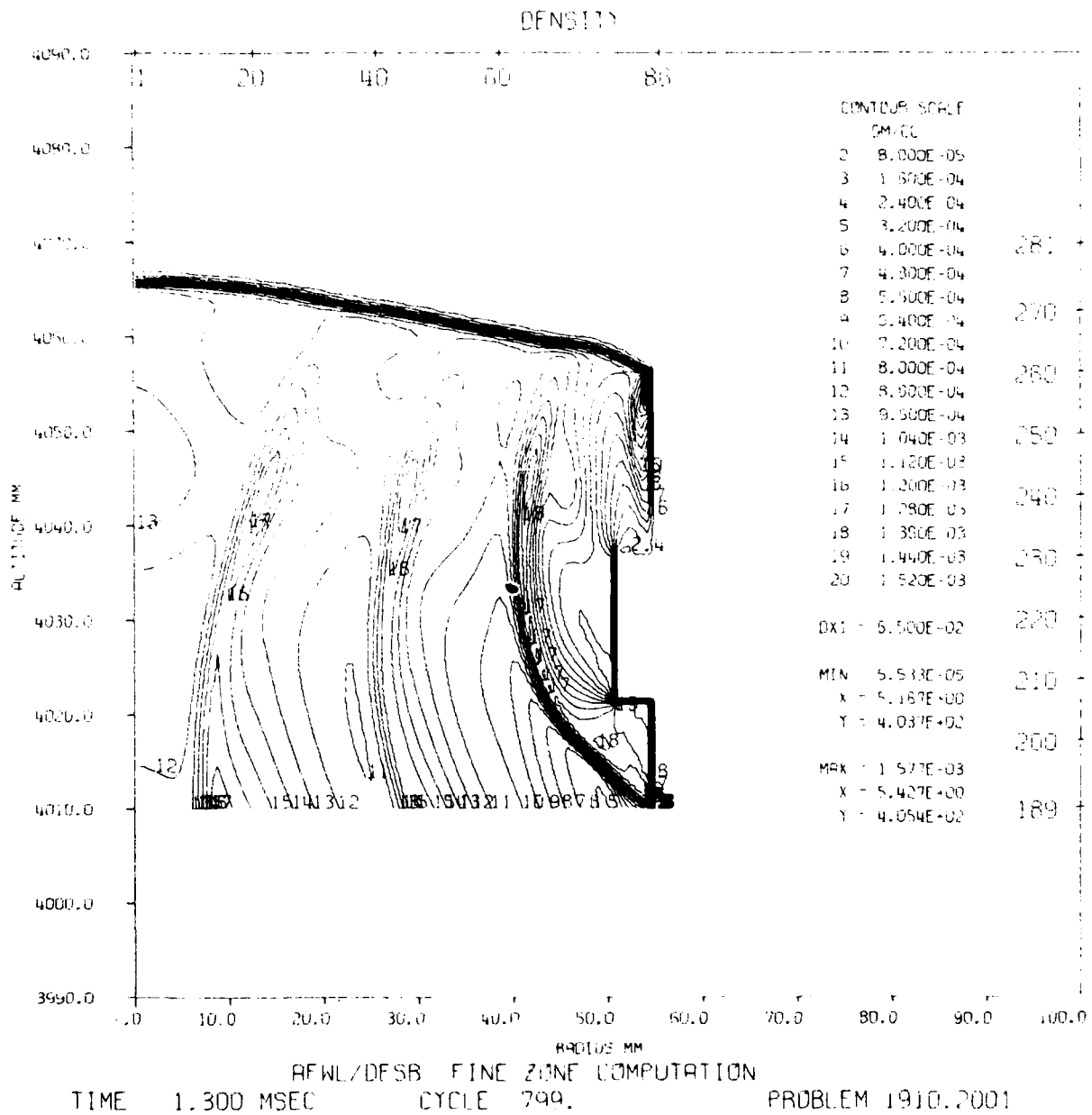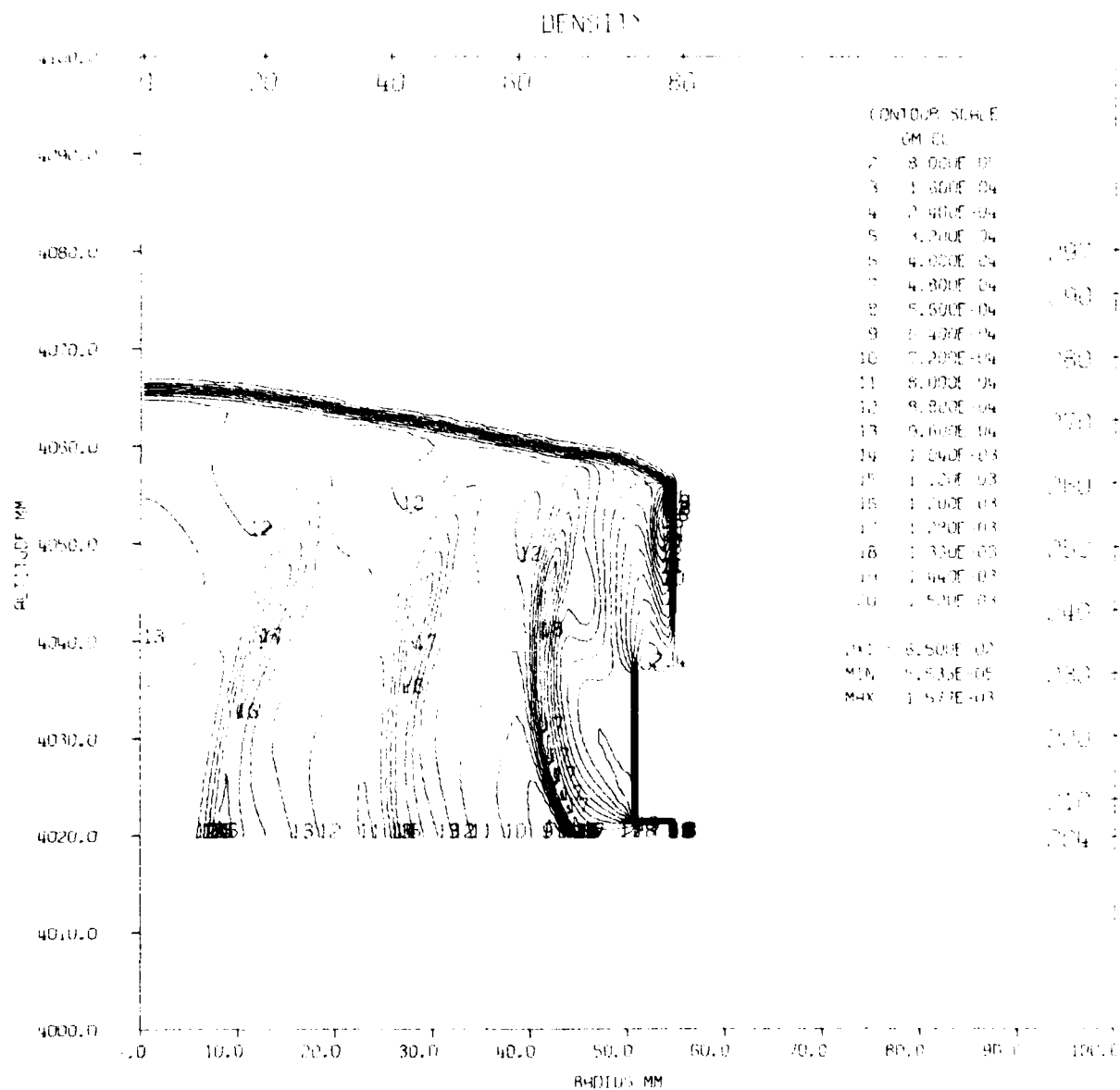
RFWL/DESB HULL CALC-RIBBED SHOCK TUBE.FINE ZONING-BERSON 1JUN78 RUN10
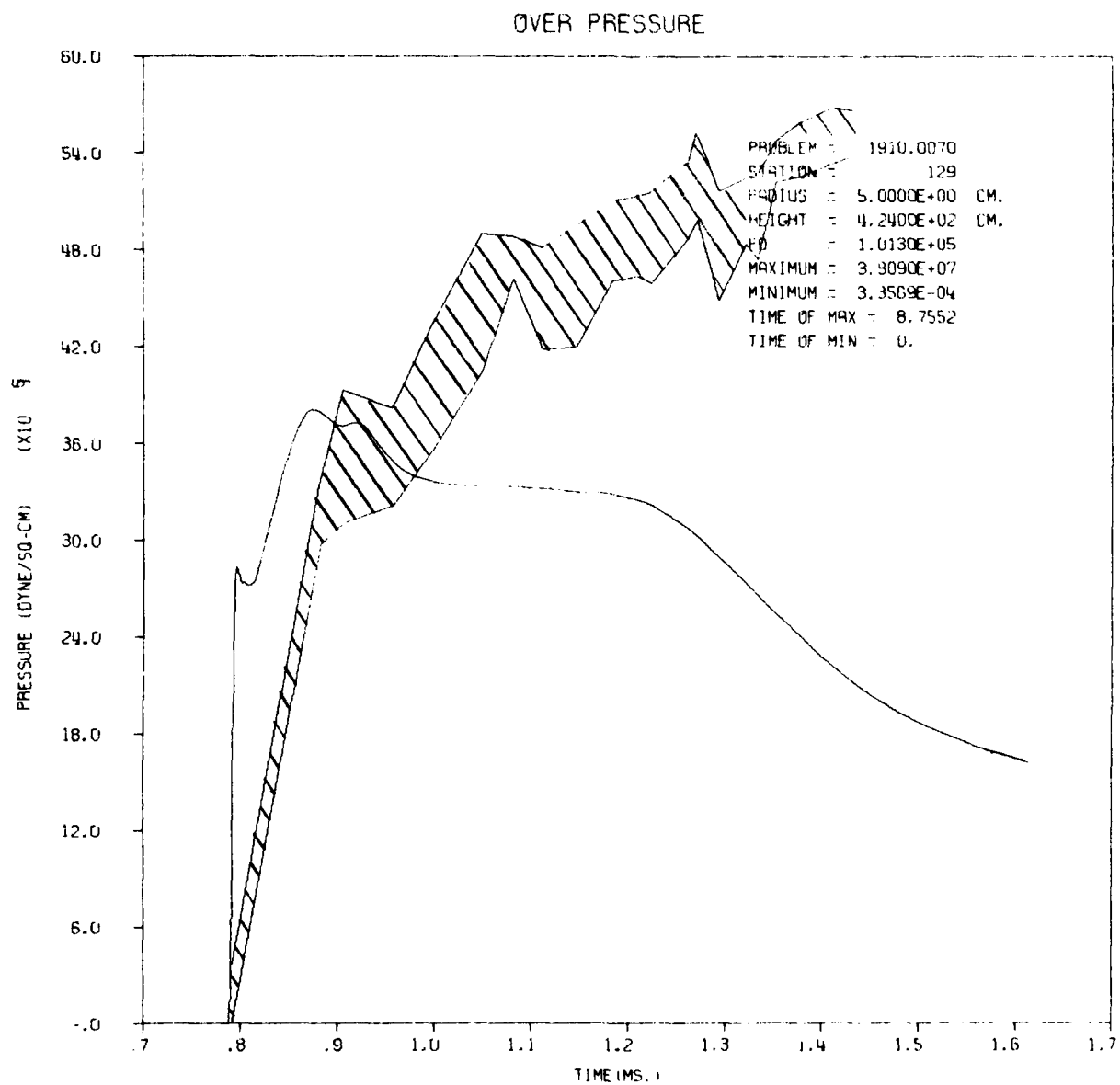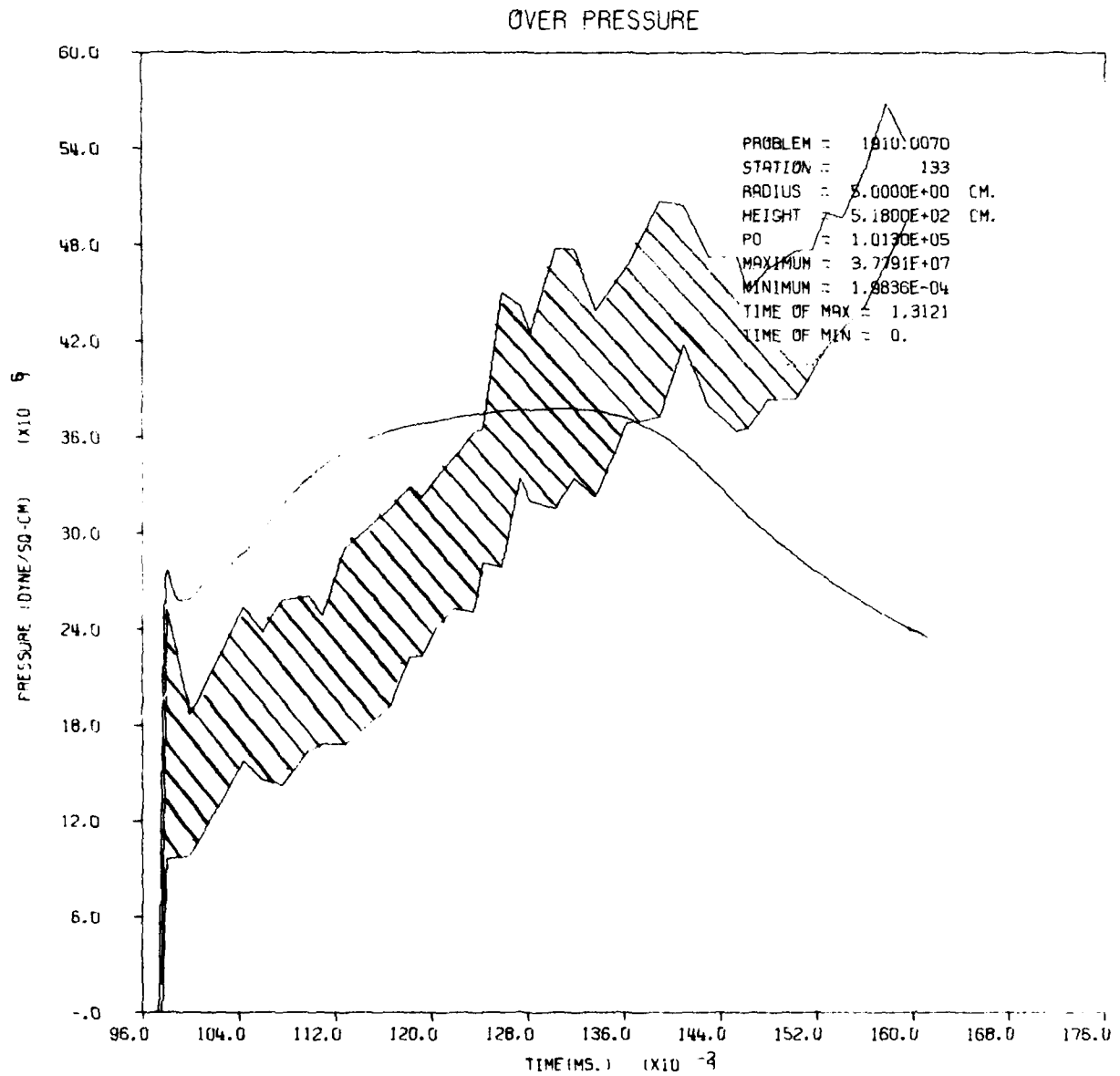TIME   1.299 MSEC   CYCLE 790.   PROBLEM 1910.2001

DENSITY

AFWL/DESR FINE ZONE COMPUTATION

TIME 1.299 MSEC   CYCLE 790.   PROBLEM 1910.2001

DENSITY

ALTITUDE MM

| | 47 | 60 | 70 | 80 | 86 |

CONTOUR SCALE
GM/CC

2	1.000E-04
3	2.000E-04
4	3.000E-04
5	4.000E-04
6	5.000E-04
7	6.000E-04
8	7.000E-04
9	8.000E-04
10	9.000E-04
11	1.000E-03
12	1.100E-03
13	1.200E-03
14	1.300E-03
15	1.400E-03
16	1.500E-03

DX1 = 6.500E-02
MIN = 1.965E-05
MAX = 1.553E-03

AFWL/DESB HULL CALC-RIBBED SHOCK TUBE.FINE ZONING-BEASON 1JUN78 RUN10
TIME 1.255 MSEC CYCLE 411. PROBLEM 1910.2001

41

DENSITY
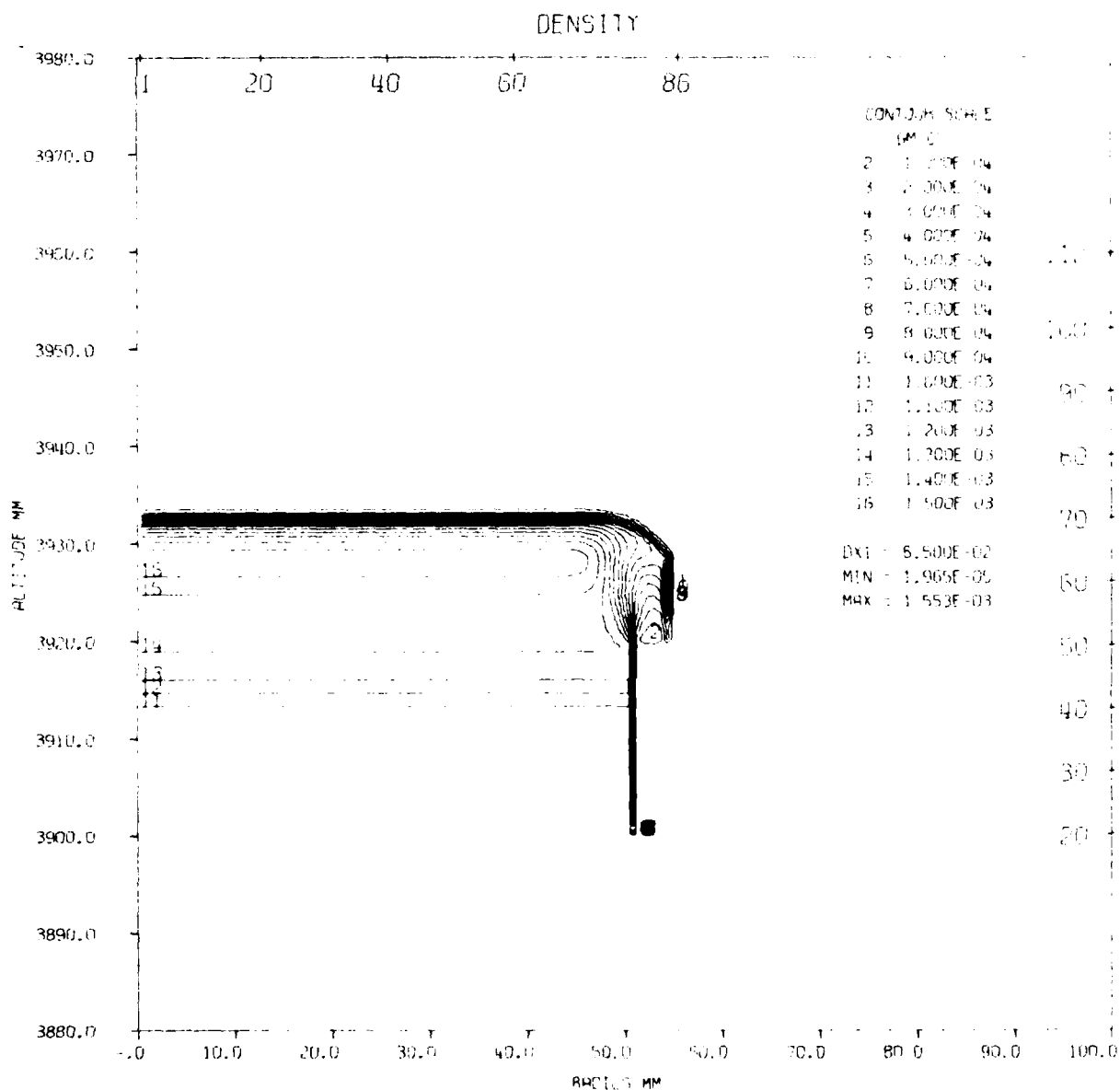
AFWL/DESB HULL CALC-RIBBED SHOCK TUBE.FINE ZONING-BEASON   1JUN78 RUN10
TIME   1.255 MSEC   CYCLE 411.   PROBLEM 1910.2001

APPENDIX B

STATION PLOTS

Station plots are the calculational equivalents of experimental sensors. At the prescribed station points, all available calculated data are recorded. The plots show the value of the hydrodynamic variables with respect to time. The following plots are station plots superimposed with digitized experimental data obtained from polaroids of SAI pressure waveforms.

OVER PRESSURE

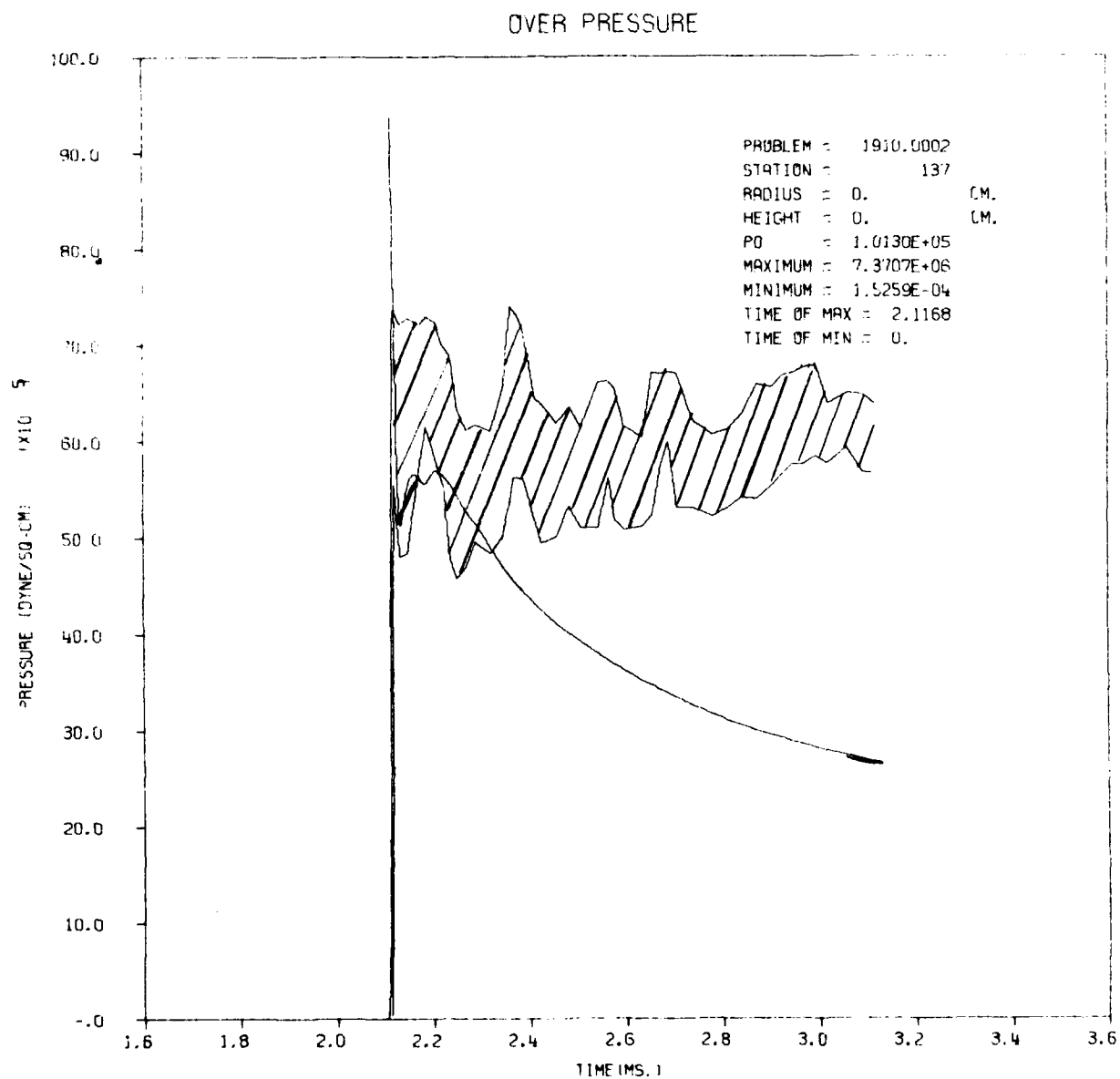

AFWL CALC-RIBBED SHOCK TUBE   PROB1910.0070-BEASON   20JUN78   RUN7 INPUT

OVER PRESSURE

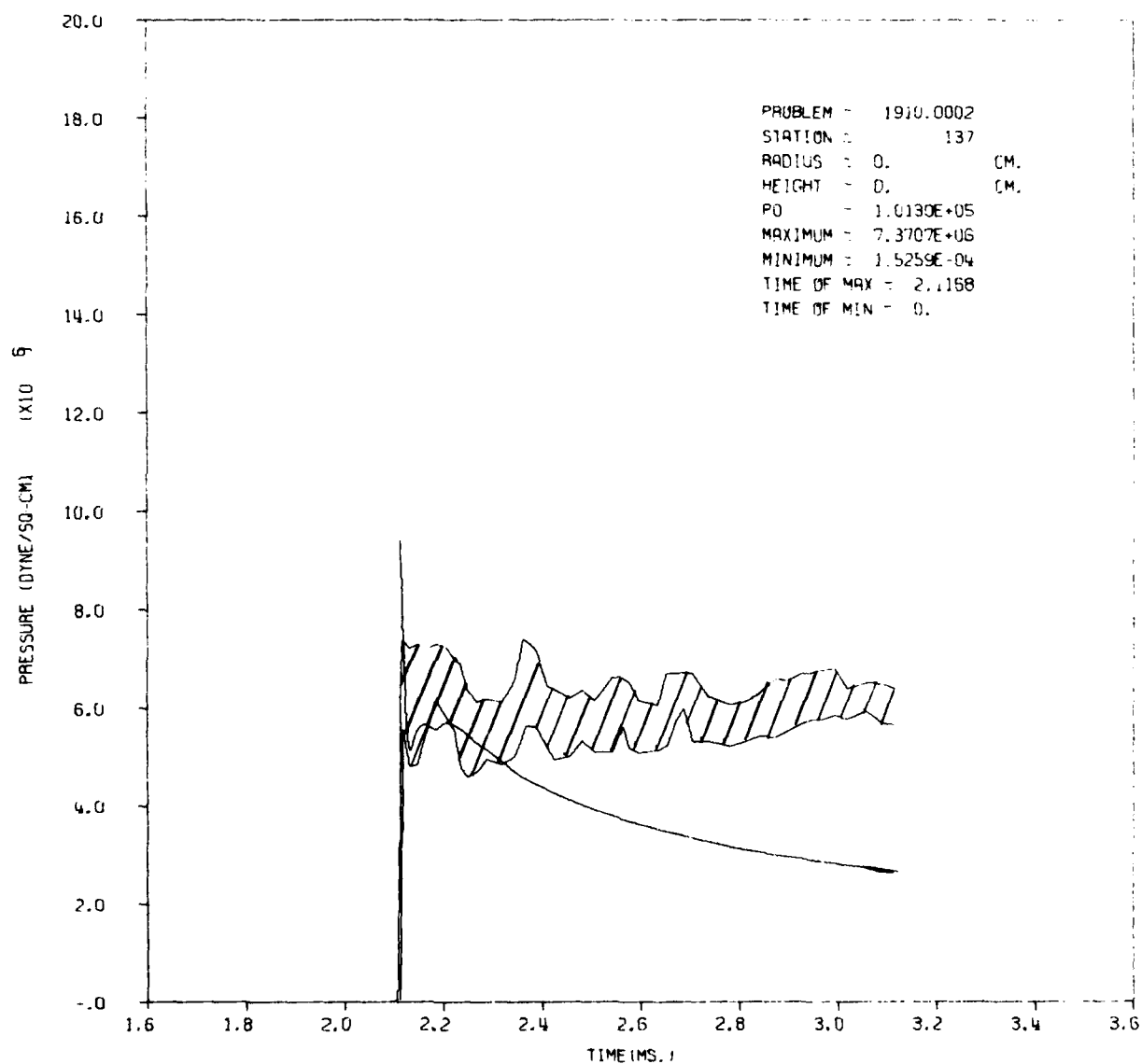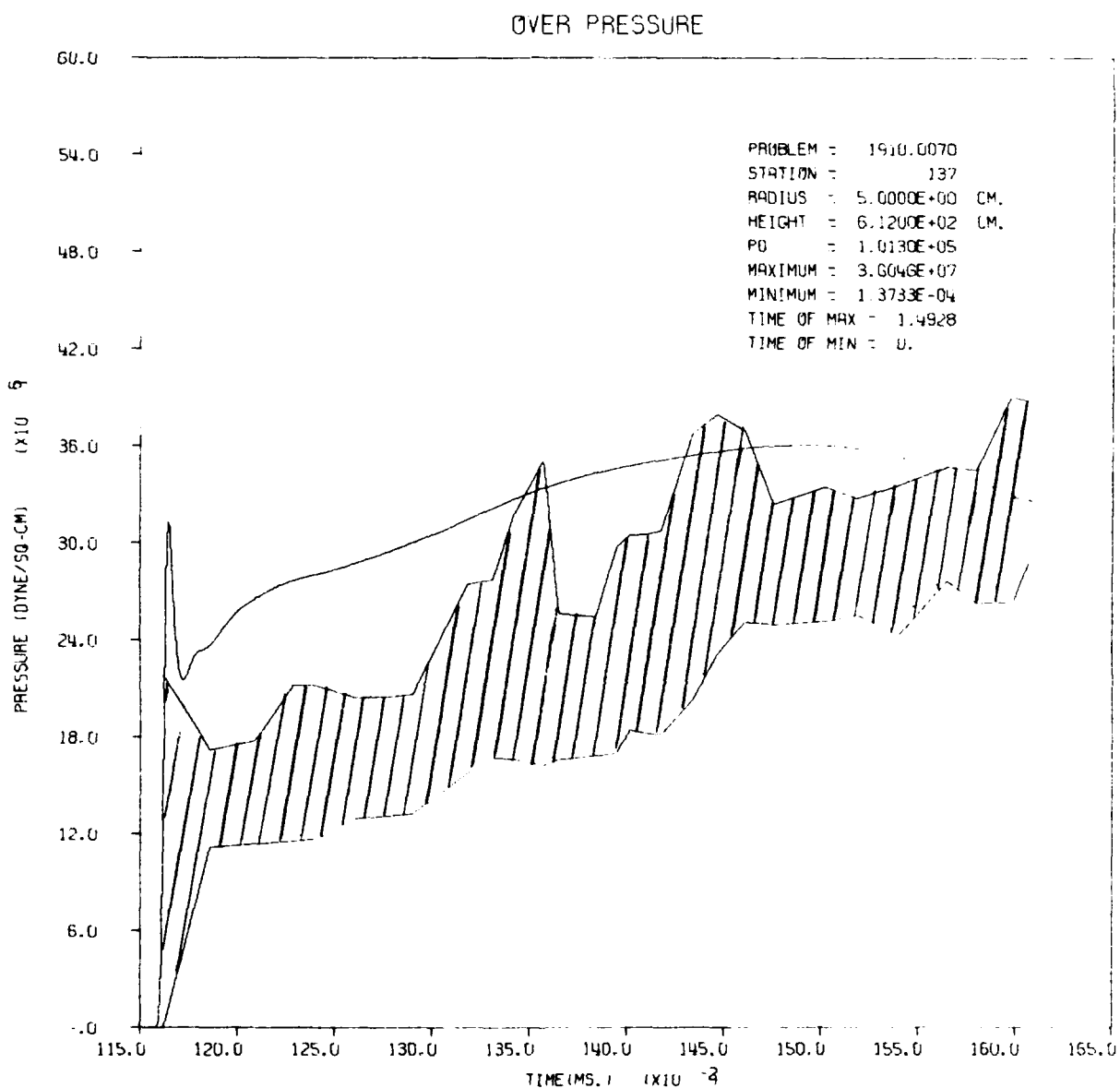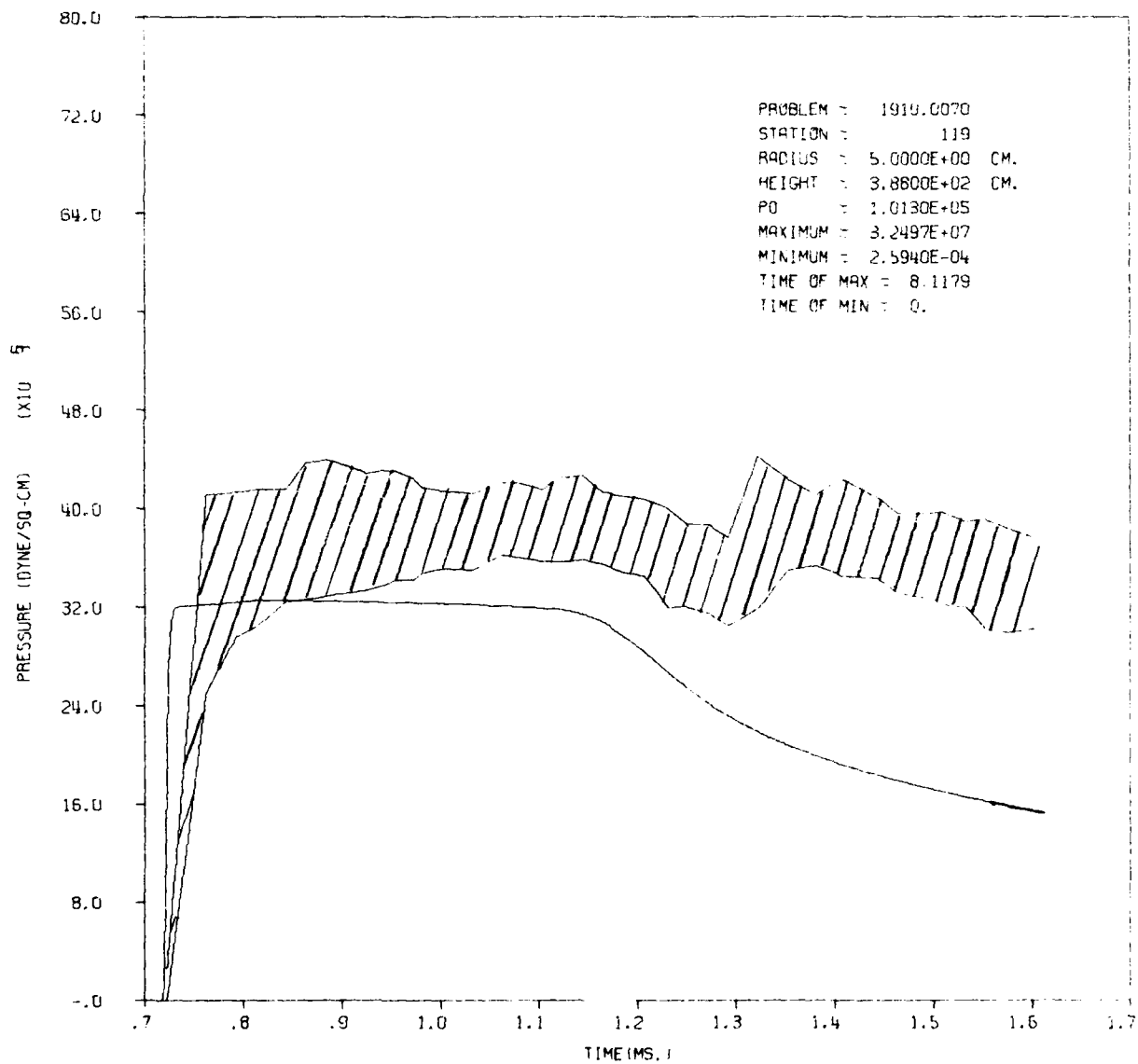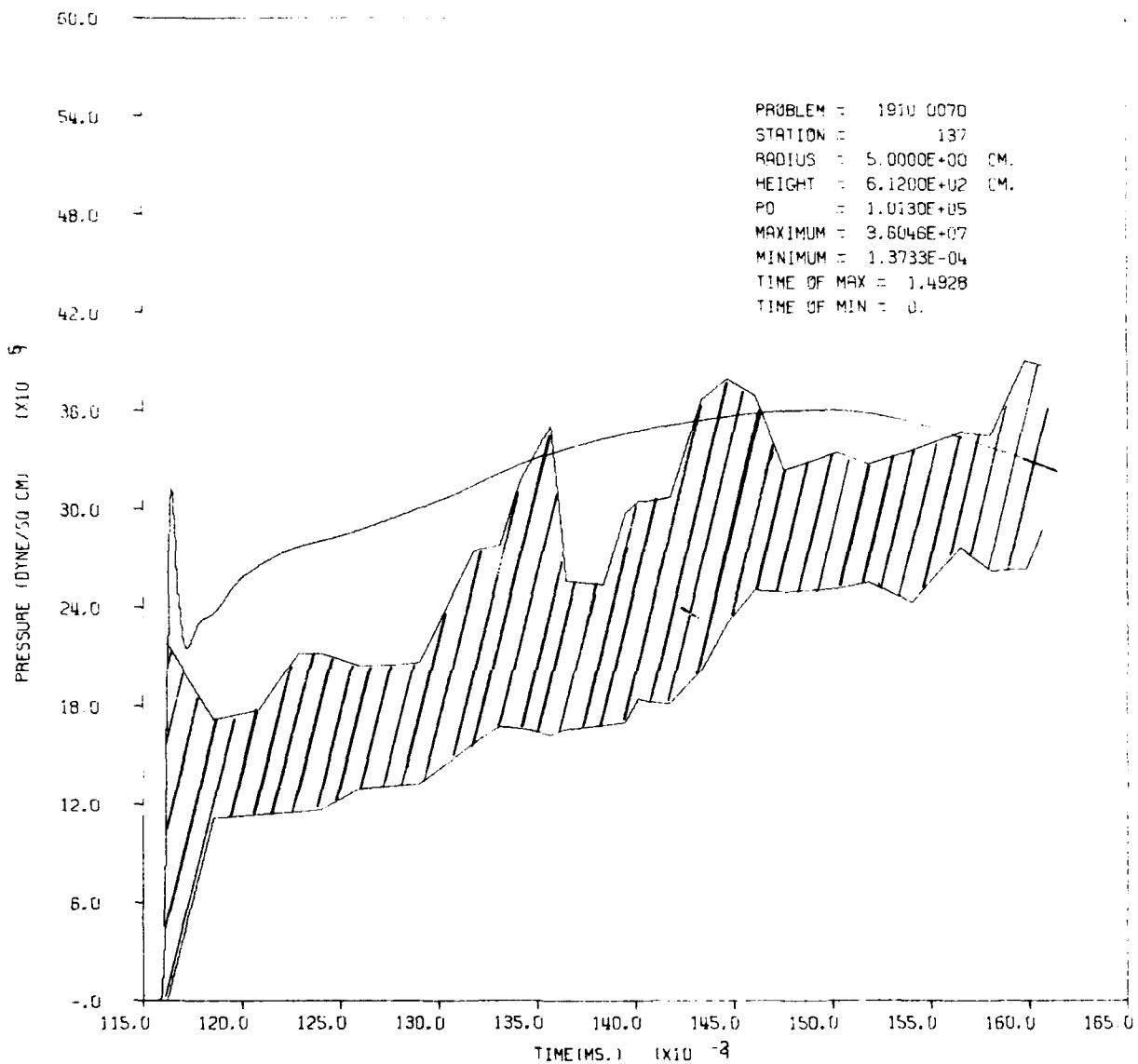AFWL CALC-RIBBED SHOCK TUBE   PROB1910.0070-BEASON   20JUN78   RUN7 INPUT

OVER PRESSURE


```
PROBLEM =   1910.0002
STATION =        129
RADIUS  =  0.         CM.
HEIGHT  =  0.         CM.
PO      =  1.0130E+05
MAXIMUM =  8.8933E+06
MINIMUM =  1.2207E-04
TIME OF MAX = 1.4174
TIME OF MIN = 0.
```

AFWL CALC-RIBBED SHOCK TUBE   PROB1910.0002-BEASON   12MAY78   RUN10 INPUT

46

OVER PRESSURE

```
PROBLEM  =   1910.0002
STATION  =        137
RADIUS   =  0.          CM.
HEIGHT   =  0.          CM.
PO       =  1.0130E+05
MAXIMUM  =  7.3707E+06
MINIMUM  =  1.5259E-04
TIME OF MAX =  2.1168
TIME OF MIN =  0.
```

AFWL CALC-RIBBED SHOCK TUBE   PROB1910.0002-BEASON   12MAY78   RUN10 INPUT

OVER PRESSURE


```
PROBLEM  -  1910.0002
STATION  :        137
RADIUS   :  0.          CM.
HEIGHT   -  0.          CM.
PO       -  1.0130E+05
MAXIMUM  :  7.3707E+06
MINIMUM  :  1.5259E-04
TIME OF MAX -  2.1168
TIME OF MIN -  0.
```

AFWL CALC-RIBBED SHOCK TUBE   PROB1910.0002-BEASON   12MAY78   RUN10 INPUT

OVER PRESSURE

PROBLEM = 1910.0070
STATION = 137
RADIUS = 5.0000E+00 CM.
HEIGHT = 6.1200E+02 CM.
PO = 1.0130E+05
MAXIMUM = 3.6046E+07
MINIMUM = 1.3733E-04
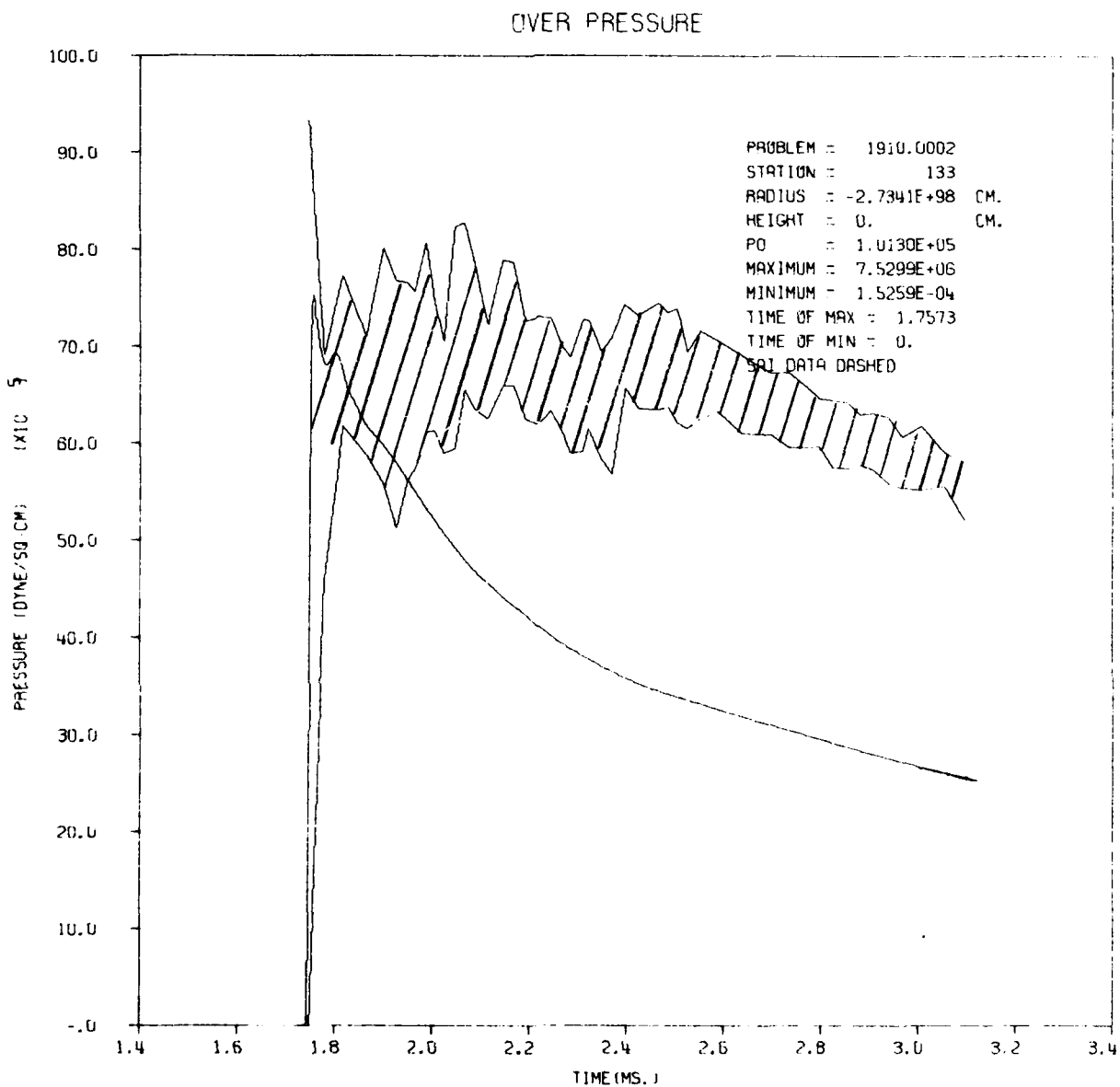TIME OF MAX = 1.4928
TIME OF MIN = 0.

AFWL CALC-RIBBED SHOCK TUBE PROB1910.0070-BEASON 20JUN78 RUN7 INPUT

OVER PRESSURE

AFWL CALC-RIBBED SHOCK TUBE   PROB1910.0070-BEASON   20JUN78   RUN7 INPUT

OVER PRESSURE

PROBLEM = 1910 0070
STATION = 137
RADIUS = 5.0000E+00 CM.
HEIGHT = 6.1200E+02 CM.
P0 = 1.0130E+05
MAXIMUM = 3.6046E+07
MINIMUM = 1.3733E-04
TIME OF MAX = 1.4928
TIME OF MIN = 0.

AFWL CALC-RIBBED SHOCK TUBE PROB1910.0070-BEASON 20JUN78 RUN7 INPUT

OVER PRESSURE

PROBLEM = 1910.0070
STATION = 119
RADIUS = 5.0000E+00 CM.
HEIGHT = 3.8600E+02 CM.
PO = 1.0130E+05
MAXIMUM = 3.2497E+07
MINIMUM = 2.5940E-04
TIME OF MAX = 8.1179
TIME OF MIN = 0.

AFWL CALC-RIBBED SHOCK TUBE PROB1910.0070-BEASON 20JUN78 RUN7 INPUT

52

OVER PRESSURE

AFWL CALC-RIBBED SHOCK TUBE   PROB1910.0002-BEASON   12MAY78   RUN10 INPUT

DISTRIBUTION LIST

<u>No of Copies</u>

1	Hq USAF, Washington DC 20330	2	BMO, Nort AFB, CA 92409

1 Hq USAF, Washington DC 20330

1 SAMI

1 XOOWD

1 PRE

1 PREE

1 RDQLM

1 RDQPN

1 RDQS

1 AFTAC/TAC, Pat AFB, FL
   32925

1 AFCEC/PREC, Tynd AFB, FL
   32401

1 AFISC/SE, Nort AFB, CA
   92409

AFSC, And AFB, Wash, DC
20331
1 DOB
1 SCS
1 DLWM

TAC, Lang AFB, VA 23365
1 LGMD
1 DERP

1 AUL/LDE, Max AFB, AL 36112

1 AU/ED, CE, Dir, Max AFB, AL 36112

AFIT, WPAFB, OH 45433
1 Tech Lib

1 CINCUSAFE, APO NY 09012

1 USAFA/DFSLB, CO 80840

SD, POB 92960, WWPC
LA, CA 90009
1 SEN

2 BMO, Nort AFB, CA 92409
   MNNH, Gage, Baran

AFWL, Kirtland AFB, NM 87117
1 HO
2 SUL
1 NT
4 NTE
20 NTES
1 DY
1 DYP

AFATL, Eglin AFB, FL 23542
1 C. Westmoreland

1 AFOSR/Lib, 1400 Wilson Blvd,
   Arlington, VA 22209

1 TAWC, Eglin AFB, FL 32544

1 Diamond Lab, Wash, DC 20438

1 RSIC/Ch, Doc Sec, Rdstn Ars,
   AL 35809

BRL, Abdn Pvg Gnd, MD 21005
1 AMXBR-TB
1 AMXBR-BL
1 AMXBR-RL

Picatinny Ars, Dover, NJ 07801
1 SMUPA-TN

USA Eng WW Exp Sta, POB 631
Vicksburg, MS 39181
1 WESRL
1 WESSS

1 WSMR/Lib, Wht Sands, NM 88002

1 Nav Ops/OP-75, Wash, DC 20305

Commander, Naval Surface Weapons Ctr.
White Oak, Silver Spring, MD 20910
1 Attn: Code F31 Tech Lib
1 J. Petes

Commanding Officer, Naval Weapons
Evaluation Facility
Kirtland AFB, Albuq, NM 87117
1 Attn: Tech Lab

Naval Research Labs
Wash, DC 20390
1 Code 2070
1 J. Boris
1 Tech Lib

Director, DNA
Wash, DC 20305
1 Attn: SPSS, G. W. Unrich
1 Attn: TITL
1 Attn: SPAS
1 Attn: RAAE

1 ODDR & E/Asst Dir, Strat Wpns,
Wash, DC 20301

1 ARPA/Lt C Whitaker, 1400 Wilson
Blvd, Arlington, VA 22209

12 DTIC/TCA, Cam Sta, Alex, VA 22314

1 DOE/Lib, Rm-J004, Wash, DC 20545

1 JSTPS/Tech Lib, Off AFB, NE 68113

1 DIA/Tech Lib, Wash, DC 20301

Sandia Lab, Kirtland AFB, NM 87115
1 Tech Lib
1 Div 5644, J. Reed
3 M. Merrit: L. Vortman: D. Dahlgren

1 LLL/Lib, B50, R134, Berkley, CA 94720

1 AFCRL/OPR, Dr. Gardiner, Hanscom AFB,
MA 01703

Sandia Lab, POB 969, Livermore, CA 94550
1 Tech Lib

LLL, POB 808, Livermore, CA 94550
1 L-51, M. Hanson
1 TID
1 Dave Glenn
1 P. Brown

LASL, POB 1663, Los Alamos, NM 87554
1 Rpt Lib
2 J-10, E. Jones: R. Gentry

Aerospace Corp, POB 92957, LA, CA 90009
1 Tech Lib
1 Dr. Harold Mirels

Brn Eng Co, 300 Sparkman, Huntsville,
AL 35807
1 Tech Lib

McDon Doug, 5301 Balsa,
Huntington Beach, CA 92547
1 Tech Lib

GE TEMPO, 816 State, Santa
Barbara, CA 93102
1 DASIAC
1 T. Barret

Kaman Sci, CO Springs, CO 80907
2 Attn: D. Sachs, Tech Lib

1 Kaman Av/J. Ruetenik, 83 2nd Ave,
Burlington, MA 01803

Mart Mar, POB 5837, Orlando, FL 32805
1 Tech Lib

MRC, 1 Presidio, Santa Barbara, CA 93102
3 Attn: R. Christian; D. Sowle; Tech Lib

SAI, POB 2351, La Jolla, CA 92307
1 Attn: Tech Lib

1 Attn: SAI/D. Hove, 101 Cont Bldg,
Ste 310, El Segundo, CA 90245
2 Attn: John Hasdal

1 Attn: SAI/Jim Craig, POB 10268
Palo Alto, CA 94303

1 Attn: GRC/J. Ise, Box 3587, Santa
Barbara, CA 93105

1 Attn: SAI/M. Torinen, Ste 808, 1901 N.
FT Myer, Arlington, VA 22209

1 Attn: SAI/Burton Chambers, 8400 Westpark
Dr , McLean, VA 22101

1 Attn: SAI/R. Clemens, 122 La Veta DR
NE, Albuquerque, NM 87108

1 Attn: BTL/W. Troutman, Whippany, NJ
07981

1 Attn: ISI/W. Dudziak, 123 W. Padre,
Santa Barbara, CA 93105

<u>No of Copies</u>

1 Attn: Rand Corp, 1700 Main, Santa Monica,   1 Attn: Official Record Copy (Lt Beason/
       CA   90406   AFWL/NTESB)

1 Attn: NASA-Langley/J. Stack, Lang Sta,   1 Attn: IDA, 400 Arm-Nav DR, Arlington,
       Hampton, VA   23365   VA   22202